Multi-criteria correlation of tephra deposits to source centres applied in the Auckland Volcanic Field, New Zealand

Jenni L. Hopkins*[a], Colin, J.N. Wilson[a], Marc-Alban Millet[b], Graham S. Leonard[c], Christian Timm[c], Lucy E. McGee[d], Ian E.M. Smith[e], Euan G.C. Smith[a].

*Corresponding author: jenni.hopkins@vuw.ac.nz

[a]School of Geography, Environment and Earth Sciences, Victoria University, PO Box 600, Wellington 6140, New Zealand

[b]School of Earth and Ocean Sciences, Cardiff University, Cardiff CF10 3AT, UK

[c]GNS Science, PO Box 30368, Lower Hutt 5040, New Zealand

[d] Department of Earth and Planetary Sciences, E&A 424, Macquarie University, Sydney, NSW 2109, Australia.

[e]School of Environment, Auckland University, Private Bag 92019, Auckland 1142, New Zealand

Manuscript revised for Bulletin of Volcanology.

Keywords

Basalt; correlation; tephra; Auckland Volcanic Field; monogenetic volcanic field; tephrochronology;

Highlights

- Outlines a method to correlate proximal whole rock samples with distal tephra deposits
- Uses this correlation with new age data to reconstruct an age order for AVF eruptions
- Discusses the spatial, temporal, and geochemical evolution of the AVF

Abstract

Linking tephras back to their source centre(s) in volcanic fields is crucial not only to reconstruct the eruptive history of the volcanic field but also to understand tephra dispersal patterns and thus the potential hazards posed by a future eruption. Here we present a multi-disciplinary approach to correlate distal basaltic tephra deposits from the Auckland Volcanic Field (AVF) to their source centres using proximal whole-rock geochemical signatures. In order to achieve these correlations, major and trace element tephra-derived glass compositions are compared with published and newly obtained whole-rock geochemical data for the entire field. The results show that incompatible trace element ratios (e.g. $(Gd/Yb)_N$, $(La/Yb)_N$, $(Zr/Yb)_N$) vary widely across the AVF (e.g. $(La/Yb)_N$ = 5 to 40) but show a more restricted range within samples from a single volcanic centre (e.g. $(La/Yb)_N$ = 5 to 10). These ratios are also the least affected by fractional crystallisation and are therefore the most appropriate geochemical tools for correlation between tephra and whole rock samples. However, findings for the AVF suggest that each volcanic centre does not have a unique geochemical signature in the field as a whole, thus preventing unambiguous correlation of tephras to source centre using geochemistry alone. A number of additional criteria are therefore combined to further constrain the source centres of the distal tephras including age, eruption scale, and location (of centres, and sites where tephra were sampled). The combination of tephrostratigraphy, $^{40}Ar/^{39}Ar$ dating and morphostratigraphic constraints allow, for the first time, the relative and absolute ordering of 48 of 53 volcanic centres of the Auckland Volcanic Field to be resolved. Eruption frequencies are shown to

vary between 0.13-1.5 eruptions/kyr and repose periods between individual eruptions vary from <0.1 to 13 kyr, with 23 of the 48 centres shown to have pre-eruptive repose periods of <1000 years. No spatial evolutionary trends are noted, although a relationship between short repose periods and closely spaced eruption locations is identified for a number of centres. In addition no temporal-geochemical trends are noted, but a relationship between geochemical signature and eruption volume is highlighted.

Introduction

The eruptive histories of basaltic volcanic fields can be reconstructed by the dating of lava and scoria deposits. These reconstructions are critical for understanding the temporal, geochemical and spatial evolution of the fields in order to better understand their potential future behaviour. However, within young fields the errors associated with current dating techniques (e.g. $^{40}Ar/^{39}Ar$ or ^{14}C) are often larger than the repose periods, and thus hinder establishment of a definitive stratigraphic age order of the centres (e.g. Briggs et al. 1994; Cook et al. 2005; Fleck et al. 2014; Leonard et al. 2017). Similarly, due to the restricted subaerial distribution of scoria and lavas from small monogenetic centres, field-wide stratigraphic relationships are often difficult to establish, and cannot resolve ambiguities that arise from the dating techniques. In these circumstances distal airfall deposits (tephras) can more reliably resolve the chronological uncertainties due to their higher preservation potential, and often stratigraphically restricted relationships.

Tephra correlation is used on a number of levels from simply correlating tephra deposit across cores or outcrops (Hopkins et al. 2015), to defining stratigraphic marker horizons (e.g. Molloy et al. 2009), or matching horizons to volcanic source or provenance through comparison of distal and proximal tephra deposit characteristics (e.g. Alloway et al. 2004; Allan et al. 2008; Zawalna-Geer et al. 2016). Linking tephras to their source volcanic centre can be straightforward where the potential number of sources is limited, the eruptive episodes (and tephras) are precisely dated, stratigraphic successions are established in proximal tephra layering, and/or the tephras (and sources) have

distinctive geochemical signatures (Lowe 2011). Where these criteria are not met, however, difficulties arise in accurately linking distal tephras to their sources. In cases where there are multiple potential sources and where proximal deposits are poorly characterised, or poorly preserved, there is currently no established method to resolve the origin of identified distal tephras.

There are a number of processes and features that should be taken into account when attempting to correlate tephra deposits. The key ones important for this study are those that can potentially produce differences in the geochemistry of glass shards in distal tephra horizons. For example, these could include atmospheric sorting of components during transportation (e.g. Lirer et al. 1973), or geochemical variation of magma produced during single eruptions (e.g. Shane et al. 2008), or the presence of micro-inclusions within individual glass shards (Lowe 2011). In addition, post-eruption processes such as reworking of deposits can produce repeated sequences (Hopkins et al. 2015), whereas poor preservation can result in inconsistent deposit thicknesses; both make the record harder to interpret (e.g. Davies et al. 2001; Pyne O'Donnell 2011). Methodological discrepancies also need to be considered. In general different sample types and size fractions are not compared (e.g. Larsson 1937), nor are analyses using different analytical methods. Many of these issues can be resolved through methodological, statistical or technical practises that we discuss below. Overall, if distal deposits could be confidently linked to their source(s), the chronology of a volcanic region could be better resolved.

The Auckland Volcanic Field (AVF) is an example of a volcanic region where climate and urbanization have resulted in the loss or obscuration of proximal tephra deposits. The spatial density of centres (53 centres distributed

over an area of ca. 600 km^2; **Fig. 1**) adds further complexity because a given tephra deposit could have come from a number of possible sources (e.g. Shane and Smith 2000). In addition, because of the rapid thinning of basaltic tephra away from source, evidence of stratigraphic successions is often limited to well preserved basinal deposits, for example in the maar crater infillings (e.g. Hopkins et al. 2015). The tephrostratigraphy of six cores from the maar craters in the AVF (Pupuke, Onepoto, Orakei Basin, Glover Park, Hopua, Pukaki; highlighted in red on **Fig. 1**) has been extensively assessed (e.g. Sandiford et al. 2001; Shane and Hoverd 2002; Molloy et al. 2009; Shane et al. 2013; Hopkins et al. 2015; Zawalna-Geer et al. 2016). The tephrostratigraphic framework developed by the careful cross correlation of the tephra deposits between individual cores, and the geochemistry of the tephra-derived glass is used as a basis for this study (e.g. Molloy et al. 2009; Hopkins et al. 2015).

Proximal lava and coarse-grained scoria cone-forming deposits in the AVF (defined here as whole-rock samples) have a higher preservation potential than proximal airfall tephra, and therefore the sources of these materials can be more easily defined (e.g. Hayward et al. 2011). In addition a large number of whole-rock analyses already exist for the AVF centres, characterising their geochemical signatures (**Table 1**). Traditional tephrochronology links distal to proximal tephra deposits, but in the AVF this process is not possible due to the lack of unambiguously sourced proximal tephra beyond the cones themselves. Here we therefore develop and present a method for correlating distal tephra (from cored maar-lake deposits, represented by glass geochemical analyses) to proximal deposits (represented by whole-rock geochemical analyses of lava or large fragments), in order to better constrain the relative and absolute eruption

history of the AVF. Here we define "tephra" as the bulk airfall deposits of material explosively erupted from the volcanoes, now found as unconsolidated pyroclastic horizons within the maar-lake cores (cf. Lowe 2011). Geochemical analyses for this study were undertaken on the juvenile glass shards derived from within these tephra horizons. The term "whole rock" is used here to refer to analyses of individual pieces of solid rock, from lava flows or from individual bombs or lapilli.

Methodology

To provide the most complete basis for tephra-to-source correlations a critical requirement is an extensive database of characteristics for all volcanic centres and tephra deposits in the field. For the AVF a large dataset already exists, including geochemistry of proximal whole-rock samples (e.g. McGee et al. 2013) and geochemistry of distal tephra-derived glass samples (e.g. Hopkins et al. 2015), ages of eruptive centres (e.g. Leonard et al. 2017), and scale of eruptions (e.g. Kereszturi et al. 2013). Currently lacking, however, is a collated field-wide suite of geochemical data of whole-rock compositions, up-to-date estimates of the ages of the tephra horizons in the maar-lake cores, and estimates of tephra volumes for the individual centres. Below we present the methods by which these pre-existing data were collated, and our new data collected.

Collation of pre-existing data

Whole-rock geochemistry for individual centres

A large amount of unpublished whole-rock geochemical data exists for the AVF. This includes datasets from MSc theses (Bryner 1991; Miller 1996; Franklin 1999; Hookway 2000; Spargo 2007; Eade 2009; see **Table 1**), and the unpublished data of I.E.M. Smith and co-workers at the University of Auckland. We also include here data from McGee (2012), the majority of which is published in McGee et al. (2011, 2012, 2013). For the newly discovered centres of Puhinui Craters and Cemetery Hill (B. Hayward *pers. comm.*), no geochemical or age data exist and therefore these centres are not included in this study. The collated whole-rock major and trace-element dataset can be found in the **supplementary material**.

Glass geochemistry for individual tephra horizons

Hopkins et al. (2015) analysed major and trace element geochemistry for glass shards from tephra horizons found in the lacustrine maar cores using Electron Microprobe Analysis (EMPA) and Laser Ablation-ICP-MS (LA-ICP-MS) at Victoria University of Wellington (VUW). Glass shards from only forty-nine basaltic horizons from five maar cores could be analysed for trace element concentrations because glass shard sizes were too small or the samples were no longer available. These data are combined with previously published major element data (Sandiford et al. 2001; Shane and Hoverd 2002; Hoverd et al. 2005; Molloy et al. 2009) reported in Hopkins et al. (2015) and outlined in the **supplementary material**.

Compatibility of pre-existing and new data

To ensure compatibility between the data sets, and as a quality control measure, we assessed the analytical methods, accuracy and precision of all data used in this contribution. For all pre-existing whole-rock analyses (outlined above), the methods and standardisation procedures were the same. XRF analyses for major elements were undertaken at the University of Auckland (UoA), and (where applicable) trace elements were analysed using laser ablation (LA)-ICP-MS on the XRF glass discs at the Australian National University (ANU). For XRF methods in-house rock standards were used (see **Supplementary Material**), and the Si concentrations obtained from XRF analysis were used for the trace element calibration. In addition duplicate analyses were undertaken by this study to ensure compatibility of the old and new data sets (see **Supplementary Material**).

For tephra-derived glass chemistry all sample preparation followed the same standard procedures. Major-element geochemistry presented in Sandiford et al (2001) was acquired at VUW on an older instrument than that used by Hopkins et al (2015); both of these studies however used wavelength dispersive X-ray spectroscopy (WDS) techniques. Data presented in Molloy et al (2009), Shane and Hoverd (2002) and Hoverd et al (2005) were obtained by EMPA at University of Auckland (UoA), using energy dispersive X-ray spectroscopy (EDS) techniques. No previous trace-element analysis had been undertaken on these samples prior to work by Hopkins et al (2015). Accuracy and precision of these methods is detailed in the **Supplementary Material**. Duplicate analyses from the same horizons, and from the same shards, were run in order to compare the newly acquired data with the existing data sets (example reported in

202 **Supplementary Material**). All aspects of these methods for both glass and
203 whole-rock analyses, and the accuracy and precision reported for the standards
204 are comparable to the methods used by this study.

205 *Ages for individual centres*

206 To maximise the amount of available age data from individual eruptive
207 centres, data from three methods have been collated. These methods include
208 morphostratigraphic evidence (e.g. Hayward et al. 2011), $^{40}Ar/^{39}Ar$ dating of
209 groundmass material (e.g. Cassata et al. 2008; Leonard et al. 2017), and ^{14}C
210 dating of organic materials contained within or bounding the volcanic deposits
211 (compiled in Lindsay et al. 2011). These are detailed in **Table 2**. Modelled ages
212 for the AVF centres suggested by Bebbington and Cronin (2011) are excluded
213 from this study, as they are based on tephra horizon ages given by Molloy et al.
214 (2009), which are superseded by those in Lowe et al. 2013 (for rhyolitic tephra
215 ages) and Hopkins et al. 2015 (for basaltic tephra horizon thicknesses and
216 depths).

217 Morphostratigraphy is here defined as the inter-relationships exhibited by
218 the surface landforms, for example where tephra or lava deposits from one
219 centre overlie another. Due to the proximity of the centres to one another within
220 the field (cf. **Fig. 1**), 35 of 53 centres have morphostratigraphic constraints
221 associated with them (outlined in **Table 2**). These morphostratigraphic
222 constraints give optimum relative ages, which need to be combined with the
223 absolute ages derived from $^{40}Ar/^{39}Ar$ or ^{14}C dating. In all cases the
224 morphostratigraphic constraints are consistent with the absolute radiometric
225 age ranges.

226 The $^{40}Ar/^{39}Ar$ ages presented in Leonard et al. (2017) are here given as age
227 ranges (the 2sd error on the age, reported in **Table 2**). This is because any age
228 within the range is considered appropriate for the centre, with no extra
229 emphasis given to the mean ages. For the 20 centres with no $^{40}Ar/^{39}Ar$ or ^{14}C
230 ages, the relative ages of 14 centres were derived by morphostratigraphy (see
231 **Table 2**). For the remaining six centres (Otuataua, Pigeon Mt., Robertson Hill,
232 Boggust Park, Cemetery Hill, and Puhinui Craters) no radiometric ages or
233 morphostratigraphic relationships are evident. As previously mentioned
234 Cemetery Hill and Puhinui Craters are not considered in this study, and therefore
235 Otuataua, Pigeon Mt., Robertson Hill, and Boggust Park are still included as
236 possible correlatives for any dated horizon during the correlation process.
237

238 ***New data acquisition***

239 *Geochemical whole rock data*

240 Prior to this study, 28 of the 53 AVF centres had three or more pre-existing
241 major and trace element analyses, fifteen centres had less than three, and ten
242 had no geochemical data at all (see **Table 1**). Volcanic centres with less than
243 three existing whole rock analyses were targeted in this study. Seventeen centres
244 had sufficient exposure to be sampled including: Boggust Park, Little Rangitoto,
245 Mt Albert, Mt Cambria, Mt Hobson, Mt Roskill, Mt Smart, Onepoto, Otuataua,
246 Pigeon Mt, Pukaki, Pukeiti, Pupuke, Mt Robertson, St Heliers, Taylors Hill and Te
247 Pou Hawaiki (**Fig. 1**). For an additional seven centres major element data existed
248 (Miller 1996), but no trace element data were reported. Thus, for these seven
249 centres (**Fig. 1**; Green Mt, Hampton Park, Mangere Mt, McLaughlins Mt,

Mclennan Hills, Mt Victoria, and Otara), samples collected by Miller (1996) were re-analysed for both major and trace elements by this study. For six centres (Ash Hill, Kohuora, Mangere Lagoon, Styaks Swamp, Cemetery Hill, and Tank Farm; **Fig. 1**), there are currently no exposures suitable for sampling (due to urbanisation and erosion), and therefore, no geochemical data exists.

Whole rock samples were crushed to <15 mm in a Rocklabs Boyd crusher, then powdered using a Rocklabs tungsten-carbide TEMA swing mill at VUW. Powders were made into fused lithium metaborate glass discs and analysed for major element oxide concentrations at the Open University, Milton Keynes, UK using X-ray Fluorescence (XRF) analysis following the methods of Ramsey et al. (1995). Internal standards WS-E (Whin Sill Dolerite) and OU-3 (Nanhoron microgranite) were analysed to monitor precision and accuracy. Major element oxides were accurate to within 2.0% of the recommended values for the internal standards and analytical precision (2σ) was 1.5% or better for all elements.

For trace element analysis, 50 mg of whole rock powder was treated using conventional methods of HF-HNO_3 digestion, and analysed on an Agilent 7500CS ICP-MS (VUW) in solution mode. Trace element abundances were calculated using the reduction program Iolite (Paton et al. 2011), using BHVO-2 as a bracketing standard, and BCR-2 as a secondary standard. ^{43}Ca was used as an internal standard using CaO contents measured by XRF. Trace element analyses were accurate to within <6% of the recommended values for the secondary standard (BCR-2) and precision (2 σ) was <6.5 % with the exceptions of Cr ±10.4 %, Nb ±22 %, Cs ±12.2 %, Ba ±11.8 %, Ta ±20.9 % and Pb ±31 %.

Tephra horizon ages

Within the Auckland maar cores as well as the locally derived basaltic tephra horizons, there are also distal andesitic and rhyolitic tephra deposits from various other sources within North Island (**Fig. 1B**). These "foreign" tephra can be used as stratigraphic marker horizons to aid both the absolute and relative dating of the basaltic deposits. The ages of the basaltic horizons within the cores are modelled by interpolating ages as a function of deposit depth, with the mean time interval per millimetre of core (**Fig. 2**). This principle assumes that tephras represent instantaneous events (Shane 2005), and therefore, their thicknesses are subtracted from the total sediment thickness. We use the most recent published ages for the rhyolitic marker horizons (RMHs; e.g. Lowe et al. 2013), and couple them with the most recent published thicknesses for the basaltic, andesitic and rhyolitic deposits in the maar cores. For basaltic deposits at Orakei and Glover Park we use data from Hopkins et al. (2015), and for the Onepoto core, all tephra thicknesses and depths are adapted from Shane and Hoverd (2002). Rhyolitic and andesitic deposit thicknesses at Orakei, Hopua, Pupuke, and lower Pukaki cores (below the Kawakawa/Oruanui RMH (Kk)) are from Molloy (2008) and in the upper Pukaki core (above Kk) from Sandiford et al. (2001).

Ages and uncertainties for all deposits found above the Maketu RMH are obtained by Monte Carlo simulation as follows. One thousand simulated sets of measured ages were found by adding the age's Gaussian noise with the standard deviations of the determined ages. Any resulting set of ages out of stratigraphic order were rejected, that is, the 1000 simulations were conditional on the ages produced being in decreasing order. The simulations were then used to produce

299 1000 sets of interpolations with the lower 5 and upper 95 percentiles of the
300 distribution giving the interpolated age uncertainties in 2σ (see **Table 3**).
301 Sedimentation rate calculations are used to estimate the ages of the
302 basaltic deposits found below the Rotoehu RMH (AVF3 to AVFc; no basaltic
303 deposits are found between Maketu and Rotoehu RMHs). The age of the Rotoehu
304 RMH itself is currently contentious, with published estimates ranging from ca. 40
305 to ca. 70 ka, associated with a range of different dating techniques (e.g. Lowe and
306 Hogg 1995; Lian and Shane 2000; Charlier et al. 2003; Wilson et al. 2007; Danišík
307 et al. 2012; Flude and Storey 2016). Here, we use an age estimate of 52 ± 7 ka
308 (D.J. Lowe *pers. comm.*), in order to accommodate the most likely range. In
309 addition, because there are no dated RMHs below the Rotoehu, these calculations
310 often assume constant sedimentation rates for a large proportion of the cores,
311 which is probably unrealistic, and thus they are taken as a guide only (**Table 3**).
312 The basaltic deposit AVFd, was used as a lower constraint for the
313 sedimentation rate between the Rotoehu and the base of the Onepoto core. This
314 deposit contains lava and scoriaceous blocks interpreted to represent the
315 Onepoto maar crater floor (Shane and Hoverd 2002). Although no age exists
316 from the Onepoto eruption, morphostratigraphy suggests that it is just younger
317 than Pupuke (Hayward et al. 2011), and we therefore use the mean age
318 measured for Pupuke (193.2 ± 2.8 ka by $^{40}Ar/^{39}Ar$ dating: Leonard et al. 2017) as
319 a maximum age for the eruption of Onepoto. The respective calculated
320 sedimentation rate of 0.19 mm/yr is comparable to those recorded previously
321 for younger core sections (0.18 mm/yr: Shane and Hoverd 2002). In addition,
322 the calculated basaltic tephra horizon ages are comparable to those calculated

for the correlated horizons AVF2 and AVF1 in the Orakei Basin core, suggesting that the assumptions made to calculate these values are realistic (**Table 3**).

In the Glover Park core, for the horizons correlated to other cores (AVF2 and AVF1), ages are assigned from an average of the values calculated from these core deposits. For horizon AVFa, which is only found at Glover Park, an age estimate was obtained through calculating the sedimentation rate between the bounding basaltic horizons, AVF1 and AVFb. The ages for these horizons were assigned based on the ages calculated for these deposits in Orakei Basin (AVF1) and Onepoto cores (AVF1 and AVFb). Calculated ages based on sedimentation rate for all basaltic tephra horizons and their associated errors are outlined in **Table 3.**

Estimated tephra volumes

Previous studies have estimated total eruptive volumes for the centres of the AVF (Allen and Smith 1994; Kereszturi et al. 2013) although, distal tephra volumes were not reported due to limited measurable material. Other studies (e.g. Kawabata et al. 2015) suggest that tephra volumes for small-scale eruptions can be estimated from the volumes of the tuff and scoria cones using the following equation:

$$V_{DRE} = 0.5V_{tuff} + 1.5V_{scoria},$$

where V is volume, and DRE is dense rock equivalent values (where volumes are corrected for void spaces, detailed in Kereszturi et al. 2013). In order to estimate tephra volume we use the most recently published DRE values for tuff and scoria from Kereszturi et al. (2013). Volume estimates are detailed in **Table 2**.

346 **Results**

347 ***Whole-rock and glass geochemistry***

348 *Whole-rock geochemistry*

349 Following the rock classification of LeMaitre et al. (2002), the AVF
350 samples range from basanitic/nephelinitic to basaltic in composition (e.g. SiO_2 =
351 39-49 wt.%; Mg# = 50-72. Broad positive trends exist between wt.% MgO and
352 wt.% CaO, and wt.% MgO and wt.% Al_2O_3. Although less obvious, there are
353 discernable broad negative trends exhibited in the AVF data between wt.% MgO
354 and wt.% SiO_2, TiO_2, $Fe_2O_3^{tot}$ and P_2O_5 (not shown). These elements are more
355 variable within a single centre than are MgO vs. CaO or Al_2O_3. For example the
356 eruptive products of Motukorea show an almost flat trend for wt.% MgO vs. wt.%
357 TiO_2,, whereas the Crater Hill samples show a strong positive trend. Although all
358 samples from the AVF seem to follow the overall major element trends on
359 variation diagrams, samples from individual AVF centres can define separate
360 trends (c.f. **Fig. 3**) within this, as previously described by McGee et al. (2013).

361 Trace-element contents in the AVF samples vary substantially, for
362 example, La 10-90 ppm, Nb 10-80 ppm and Sr 300-1000 ppm (see
363 **Supplementary Material**). Similar to the major elements, some of the trace
364 elements show overall general trends for the field, as well as trends specific to
365 each centre (**Fig. 3**). There is a strong positive trend for wt.% MgO and ppm Cr
366 and Sc, and a general negative trend of variable slop exists between wt.% MgO
367 and ppm Th, Nb, Sr, and La (**Fig. 3**).

368 Mantle-normalised trace-element data for near primitive AVF samples
369 (e.g. Mg# ≥ 60) are broadly similar and are characterised by a positive Nb

anomaly and a negative sloping light to heavy rare earth element profile (e.g. La/Yb range 4 to 40; **Fig. 4**), characteristics that are similar to ocean island basalts (OIBs). Some centres (e.g. Rangitoto 2 and Te Pou Hawaiiki) have geochemical signatures that are less enriched in trace elements than others, characterised by a shallower rare earth element (REE) pattern gradient (e.g. La/Yb ≤ 7.5), and a positive Sr anomaly (e.g. Sr* ≥ 1.2). In contrast, samples from trace element-enriched centres (e.g. Mt Cambria, Mt Hobson, St Heliers) have a relatively steep REE pattern gradient (e.g. La/Yb ≥ 20), show a small trough at Zr-Hf, exhibit no Sr anomaly (e.g. Sr* ≤ 1.0), and display a negative K anomaly (e.g. K* ≤ 0.7; **Fig. 4**). These major and trace element signatures for the field are discussed in detail by McGee et al. (2013), and are attributed to mixing during ascent of magma from three mantle sources.

Glass geochemistry

The geochemical composition of glass shards found in the AVF tephras are discussed in detail in Hopkins et al. (2015; see Fig 4 therein). In general they show a consistent range in MgO (ca. 2 to 7.5 wt.%), CaO (ca. 7 to 15 wt.%), FeO (ca. 9 to 15 wt.%), K_2O (ca. 1 to 4 wt %), and TiO_2 (ca. 2 to 4.5 wt.%) between samples from across all cores. Al_2O_3 concentrations are shown to be consistently lower at given MgO values in the Orakei and Onepoto cores, and SiO_2 is consistently lower at given MgO values in the Onepoto core. Glass shards from individual horizons have mostly similar major element concentrations with variations within <1 wt. % for MgO, SiO_2, FeO, and TiO_2, and <3 wt. % for CaO, Al_2O_3, Na_2O, and K_2O, with minor numbers of horizons showing bimodal or

systematic ranges in concentrations of major elements (as discussed in Hopkins et al. 2015).

In addition to major oxides, Hopkins et al. (2015) analysed trace elements on individual ≥30 μm diameter glass shards. Their results showed (similar to whole-rock analyses) high variability in concentrations for trace elements, for example La ca. 5-100 ppm, Nb ca. 20-175 ppm, and Sr 140-1500 ppm. In general, glass shard primitive-mantle normalised multi-element plots show comparable signatures to the whole rock geochemical patterns (**Fig. 4**). Glass shards from individual tephra horizons have a more limited range in trace-element concentrations when compared to the whole field, and in many cases show relatively distinct trace element patterns for each individual tephra horizon (**Fig. 4**).

Tephra horizon ages

Age estimates for all tephra horizons used in this study are outlined in **Table 3** and summarised in **Figure 2**. Basaltic tephra horizons found within 6 cores span a large age range in the field from 0.54 to ca. 143 ka (AVF24 in Pupuke core and AVFc in Onepoto core respectively). Fourteen horizons have ages calculated at <28 ka, nine horizons are found between ca. 28 and 35 ka, and only 6 horizons have ages of ca. 59-143 ka. Overall the estimated ages are in good agreement where multiple deposits are correlated across cores (**Fig. 2**). Two discrepancies, however, arise (highlighted in **Table 3**): 1) The calculated age for AVF17 appears too young within the AVF number sequence, and 2) the calculated age of AVF16 appears too old for the AVF number sequence and

417 suspiciously similar to the age of AVF13. These results are potentially
418 problematic, and are therefore discussed below.

419 The age of AVF17 when estimated using only the Orakei Basin core (23.35
420 ka), rather than averaging all ages across the cores, is not chronologically out of
421 place (e.g. AVF18 is 23.2 ka and AVF15 is 24.5 ka). However, using the average
422 age for AVF18, which is calculated as the average of correlated units from
423 multiple cores (deposits from within Hopua 25.2 ka, Pukaki 24.6 ka and Orakei
424 23.35 ka cores) it appears too old (**Table 3**). This is because the ages for the
425 deposits in the Pukaki and Hopua core are slightly older than those estimated
426 for just the Orakei Basin core. But, within this section (Okareka to Te Rere), all
427 of the horizon ages calculated are within error of each other, and therefore
428 stratigraphic constraints in the cores are required to resolve the absolute
429 ordering. AVF19 is found above the andesitic horizon Eg36 (**Fig.** 2; Molloy
430 2008), which is found in all the cores, and therefore acts as a marker horizon to
431 place AVF19 as the youngest horizon. AVF18 is found above AVF17 within the
432 Orakei Basin core, further restricting the ordering of these two horizons. The
433 ordering and correlation of these horizons will therefore be maintained,
434 however, the errors on the ages must be taken into account during the
435 correlation process.

436 The ages calculated for AVF16 (Pukaki core only) and AVF13 (Orakei core
437 only) are identical (25.23 ± 0.86 ka and 25.23 ± 0.31 ka respectively). The age
438 estimate for AVF16 implies that it is older than suggested by the original
439 position in the AVF nomenclature sequence, and there is a strong possibility that
440 the horizons represent the same deposit. Stratigraphically, there are limited
441 constraints on the relationship of AVF16 with the other deposits from other

cores. The andesitic deposit Eg34 is found below AVF16 but is not found in any other cores and therefore provides no further regional stratigraphic constraints. The Te Rere and the Kawakawa/Oruanui RHMs stratigraphically constrain horizon AVF16 (above and below respectively), but there are no other age constraints (Te Rere tephra is not found in the Orakei Basin core). In addition there are limited geochemical data for the deposit AVF16 to confirm or deny its relationship with AVF13 (Sandiford et al. 2001; Hopkins et al. 2015). Therefore due to the lack of distinct evidence to suggest these deposits are not the same, and the overwhelming similarity in the ages, we assume AVF16 and AVF13 record the same event and will be referred to as 'AVF13' with an age of 25.23 ± 0.86 ka in the following discussion.

Discussion

Discriminatory geochemical elements for the AVF

Previous studies on the petrogenesis of AVF eruptive products have shown that each magma batch feeding a single centre is generated by mixing of contributions from differing degrees of partial melting of multiple mantle sources at different depths (Huang et al. 1997; McGee et al. 2013, 2015; Hopkins et al. 2016). The resulting geochemical signatures of the erupted volcanic products demonstrate that although there is overlap for many elements, combinations of some major element (SiO_2, MgO, CaO, FeO, P_2O_5) and trace element (Sc, Sr, Zr, Gd, La, Sm, Nd, Nb, Ce) concentrations or ratios (e.g. $(La/Yb)_N$ or $(La/Y)_N$) can be used to discriminate single trends for individual centres (**Fig.**

465 **3**). The selected elements also show the widest range in concentrations in
466 eruptive products from the AVF.
467 The rare-earth elements (REEs) are especially useful because fractional
468 crystallisation of the common silicate phases has only a minor effect on their
469 concentrations. They can therefore be used to discriminate between melts from a
470 deep (garnet-bearing mantle = high light REE/heavy REE) or shallow (spinel-
471 bearing mantle = low light REE/heavy REE) source (e.g. McKenzie and O'Nions
472 1991; Robinson and Wood 1998; McGee et al. 2013, 2015; Hopkins et al. 2016;
473 McGee and Smith 2016). As a result of these variations, and of the discriminatory
474 nature of certain elements and element ratios within the AVF, we show that
475 geochemical fingerprinting can be used as a method to correlate distal tephra
476 deposits to their source centre. Below we discuss the techniques by which this
477 method was tested and developed.
478
479 ***Geochemical correlation***
480 A key issue in correlating the geochemistry of glass shards in distal tephra
481 to whole-rock geochemistry of proximal lavas and pyroclastic particles is that
482 most whole-rock samples contain mineral inclusions (e.g. olivine), whereas small
483 volcanic glass shards (in tephra) do not. Hence, the concentration of elements
484 that strongly partition into mineral phases (e.g. Mg, Ni or Cr into olivine) in
485 whole-rock samples will not be comparable to the respective element contents in
486 the glass shards (e.g. **Fig. 5A**). Conversely, elements that preferentially remain in
487 the melt (e.g. those that are incompatible with mineral phases commonly found
488 in alkali basalts, such as the REE) are likely to have comparable concentrations in
489 whole-rock and glass shards. In addition, mineral-free groundmass glass from

490 whole-rock samples is likely to have a comparable geochemical signature to the
491 glass shards forming distal tephra deposits (e.g. Lowe 2011; Allan et al. 2008;
492 Lowe and Alloway 2015; **Fig. 5B**).

493 These hypotheses were tested initially on samples from a known source by
494 comparing the geochemical composition of (a) a proximal whole-rock sample
495 and (b) the matrix-derived glass from that sample to (c) glass shards from a
496 distal tephra deposit. The whole-rock lava sample Mt. Wellington AU62394 was
497 chosen for two reasons, 1) it has a fresh, glassy groundmass and, 2) distal tephra
498 from Mt. Wellington has been unambiguously identified in the Hopua core based
499 on age and thickness (Molloy et al. 2009). The lava sample was processed first as
500 a whole-rock sample (XRF and ICP-MS, see methodology). It was also processed
501 to produce a 'matrix-derived glass' sample by crushing the rock and separating
502 shards of matrix glass that were of comparable size (30-100 μm) to the glass
503 shards found in the tephra horizon from the Hopua core (Molloy et al. 2009).
504 These separated matrix-derived glass shards were then analysed by EMPA and
505 LA-ICP-MS using methods outlined in Hopkins et al. (2015).

506 *Geochemical correlation of glass shards from distal tephra deposits with matrix*
507 *derived glass*

508 **Figure 6** shows MgO vs. Al_2O_3 (in wt. %. [**Fig. 6A**]) and Gd vs. Zr (in ppm
509 [**Fig. 6B**]) for matrix-derived glass and the glass from its known distal correlative
510 from the Hopua core, the overlap in the data demonstrates that their
511 compositions are comparable. This is the case for a wide range of both major and
512 trace elements (including, MgO vs. full major element suite plus trace elements
513 Rb, Zr, Cs, Ni, Cr, Y, and Er; SiO_2 vs. Al_2O_3, Na_2O, K_2O, and CaO vs. Al_2O_3, Na_2O).

514 Limited variability exists between trace elements (e.g. Rb, Zr, Ni, Cr and Y, and
515 the REE) when plotted against each other, or against Al_2O_3 or MgO.
516 For some elements, however, the glass from the distal tephra has larger
517 variations than does the matrix-derived glass (**Fig. 6A**). This is attributed to
518 either 1), the matrix-derived glass being made from a single clast and thus
519 having minimal compositional variation, and/or 2) glass shards from the distal
520 tephra showing a higher variability due to initial differences in composition of
521 the erupted magma creating variability in the glass shard composition
522 throughout the eruption (e.g. McGee et al. 2012). This test proves that matrix-
523 derived glass from proximal samples can be successfully correlated with glass
524 shards in distal tephras using trace elements and trace element ratios (**Fig. 6B)**.
525 Geochemical analysis using EMPA and LA-ICP-MS techniques are for
526 individual glass shards, ensuring phenocrysts and microlites are not analysed.
527 Accordingly matrix-derived glass from proximal samples can be correlated with
528 glass shards from within distal tephra deposits using both elements that are
529 highly compatible and elements that are incompatible. Compatible elements are
530 preferentially incorporated in key crystallising minerals within the whole rock
531 (e.g. olivine) and therefore result in comparable glass chemistries between
532 matrix-derived glass and tephra-derived glass. The incompatible trace elements
533 can also be used because they are not preferentially taken into the crystal
534 phases. We therefore conclude that matrix-derived glass from whole-rock
535 samples can be correlated to glass shards from the distal tephra deposits, with
536 some minor caveats. For example, this method relies on the existence and ability
537 to extract glass from the groundmass of proximal whole-rock samples, which is
538 not always possible.

539 *Correlation of glass shards from distal tephra with whole-rock samples*

540 In general, when the entire suite of whole-rock and glass geochemical
541 datasets are compared, MgO, Cr, and Ni all show distinctly higher concentrations
542 in whole-rock samples than in the glasses (e.g. MgO in whole rock range from ca.
543 6-16 wt.%; in glass ca. 2-6 wt.%: **Fig. 5A**). Compared to whole-rock analyses, all
544 glasses contain higher (but slightly overlapping) wt.% SiO_2, Al_2O_3, Na_2O, and K_2O
545 contents (e.g. SiO_2 in whole rock ca. 38-50 wt.%; glass ca. 42-52 wt.%). CaO, FeO,
546 TiO_2, and P_2O_5 have comparable ranges between whole rock and glass, as do the
547 trace elements, including REEs (**Fig. 5B**). The REEs in general do show
548 comparable but slightly wider ranges in concentrations in the glass than in the
549 whole rock (e.g. Sr in glass = 140-1500 ppm vs. Sr in whole-rock = 300-1000).

550 In addition to the presence of phenocrystic material combined into a bulk
551 rock analysis, correlating major-element compositions of proximal whole-rock
552 samples to those of glass shards in distal tephra has proved difficult, due to the
553 effect that fractional crystallization has on the concentrations of some elements
554 (e.g. Pearce et al. 2008; Ukstins Peate et al. 2008; Dunbar and Kurbatov 2011;
555 Óladóttir et al. 2012). Plotting element concentrations (for whole-rock samples
556 from a single centre or glass shard analyses from one tephra horizon) against
557 other elements that are compatible with certain crystals (e.g. MgO for olivine,
558 CaO and Al_2O_3 for pyroxene or plagioclase) can be used to monitor the effect of
559 crystal removal on these elements in the glass. If an element shows a positive or
560 negative correlation ($r^2 \geq 0.6$, where no single point is responsible for the trend),
561 with key compatible major elements (MgO, CaO, Al_2O_3) then that element is
562 significantly affected by crystal removal and therefore not useful for correlation
563 purposes. In addition to key major elements, trace elements with high partition

564 coefficients for olivine and pyroxene (e.g. Ni, Cr, Sc) are also affected. For
565 example, **Fig. 7** shows that for MgO vs. Ni, the whole rock $r^2 = 0.75$, and for
566 tephra-derived glass $r^2 = 0.61$. Conversely, high field strength elements (HFSE),
567 such as Nb, Zr, and REE, show no trend with elements tracing fractional
568 crystallisation (e.g. for MgO vs. La; $r^2 = 0.02$ for tephra-derived glass, and $r^2 =$
569 0.11 for whole rock. This exercise discussed above was repeated for all glass-
570 shard analyses from all tephra horizons and for all whole-rock samples from all
571 centres using MgO, CaO, Al_2O_3, Ni, Mn, and Sr on the x-axis (and all other major
572 and trace elements on the y-axis). These results suggest that HFSEs are
573 incompatible with major crystallising phases and are therefore well suited for
574 geochemical fingerprinting (e.g. **Fig. 6E-F; Fig. 7**). Respective trace element
575 ratios (e.g. $(La/Yb)_N$, $(Gd/Yb)_N$, $(Zr/Yb)_N$, $(Ce/Yb)_N$, $(Nb/Yb)_N$, and $(Nd/Yb)_N$) also
576 showed no correlation with any of the x-axis elements. Therefore, these ratios
577 are considered best for geochemical correlation between glass shards and whole
578 rocks. Such ratios show a broad range in the AVF as a whole, but a relatively
579 restricted range in samples from each single centre, and no relationship with
580 indices of fractional crystallisation.

581 When applied to the known Mt Wellington samples, a comparison of
582 proximal whole rock, matrix-derived glass (of the same whole rock sample), and
583 distal tephra-derived glass show the expected results. **Figure 6C** shows an
584 example of element combinations that are comparable for glass-glass
585 correlations but not for glass-whole rock correlations (e.g. MgO vs. Al_2O_3, K_2O, Ni,
586 Cr, and the REE). In contrast, some major element combinations do appear to
587 correlate the whole-rock with glass of the distal tephra (**Fig**. **6D;** including SiO_2
588 vs. TiO_2 and FeO, and CaO vs. TiO_2, FeO and Al_2O_3). In these cases, however, the

589 strong correlation is mainly due to the small variability observed in the Mt
590 Wellington samples; it may not be applicable for other centres within the AVF.
591 **Figure 6E** illustrates an example of incompatible trace elements in glasses that
592 show slightly more variability than the whole-rock samples do; this discrepancy
593 is, however, minimised when trace element ratios for the two sample types are
594 compared (see **Fig. 6F**). The incompatible trace element ratios are sufficiently
595 distinctive to allow independent correlation to be made between the field-wide
596 suite of proximal whole-rock and distal glass data, especially $(La/Yb)_N$, $(Gd/Yb)_N$,
597 and $(Zr/Yb)_N$, all of which show a wide range of values in the field as a whole. It
598 is therefore concluded that by using incompatible-element and LREE/HREE
599 ratios, it is possible to geochemically correlate individual glass shards from distal
600 tephra deposits with proximal whole-rock samples. There are, however, some
601 additional limitations for the AVF.

602 *Limitations on geochemical correlations*

603 Previous studies have demonstrated that the geochemical composition of
604 the erupted products within some of the AVF centres (e.g. Crater Hill: Smith et al.
605 2008; Motukorea: McGee et al. 2012), change as the eruptions progress from
606 initially phreatomagmatic to magmatic eruption styles (**Table 2**). These centres
607 consistently show, for example, initially low wt.% SiO_2 and Mg/Fe ratios and
608 higher incompatible element contents that evolve to final products with higher
609 wt.% SiO_2, Mg/Fe ratios and lower incompatible element abundances (e.g.
610 Reiners 1998; Smith et al. 2008; McGee et al. 2012). Such variability may
611 complicate correlation of proximal units to their related distal tephra deposits

612 because directions and distances of eruptive dispersal may not be constant
613 through an eruption.

614 For AVF centres, most of the eruptive phases are explosive (**Table 2**), and
615 therefore, if centres show geochemical evolution through an eruption (e.g.
616 Motukorea, Crater Hill), there is the potential for tephra deposits (from early
617 phreatomagmatic phases) to have higher trace element ratios (LREE/HREE)
618 than their subsequent lava or scoria deposits (from later magmatic phases). This
619 bias may hinder correlation of some distal tephras to their source centre.

620 To address this issue, **Fig. 8** shows the geochemical progression through
621 the eruption of Motukorea (data from McGee et al. 2012), compared with the
622 correlated Motukorea tephra horizon found in the Orakei Basin core. Distal
623 tephra-derived glass shards appear to show slightly higher SiO_2 concentrations
624 at given Zr concentrations (due to fractional crystallisation processes), but do
625 show the full evolutionary geochemical trend for the entire eruption. For the
626 incompatible trace element ratios the glass shards appear to be geochemically
627 comparable and again have signatures that are the same as all phases of the
628 eruption from tuff (explosive early phases), to lava and scoria (less-explosive
629 later phases) (**Fig. 8**). Although these results generally validate our method, we
630 still cannot discount the possibility of a mismatch, due to the limited geochemical
631 data available for the evolution of individual centres.

632 Another limitation of using geochemistry to correlate tephras to their
633 source centres is that not all the 53 AVF centres show distinct geochemical
634 signatures. Geochemical composition alone cannot unambiguously fingerprint a
635 centre if there are either a large number of centres with relatively similar
636 geochemical compositions, or a general lack of geochemical data (either whole

637 rock or glass). It is therefore essential to include additional criteria (discussed
638 below) to allow confident correlations to be made.
639

640 ***Multi-criteria correlation of tephra horizons to source centres***

641 We combine four key factors to correlate distal tephra deposits to their
642 source centres: age, geochemistry, scale of eruption, and location of sources.
643 Where applicable, wind direction is also taken into account.

644 A shortlist of potential source centres (**Table 2**) is created based primarily on
645 the restrictions provided by the age estimates of the tephra deposits and the age
646 estimates of the centres. For those shortlisted centres, the major, trace, and trace
647 element ratios of the proximal whole rock analyses are compared to the distal
648 tephra derived-glass compositions, focussing on incompatible trace element
649 ratios (**Fig. 9**). To strengthen potential correlations, other criteria such as the
650 eruption scale and styles, and the location of the relevant source centre(s), and
651 the relevant core(s) are also taken into account, as discussed below.

652 Because fall deposits thin systematically with distance (Pyle 1989; Lowe
653 2011), eruptions with a large estimated tephra volume (ETV) and a dominant
654 phreatomagmatic component are likely to produce a larger tephra output and
655 hence a greater dispersal footprint and deposit. Therefore, very thick (primary)
656 tephra deposits (>100 mm) in a core (Hopkins et al. 2015) require a source
657 centre that is either 1) close to the deposition site (less than a few kilometres:
658 Brand et al. 2014), and/or 2) has a predominantly phreatomagmatic eruption
659 style, and/or 3) has a large magma supply and thus a long eruption duration.

660 Due to the relatively small size of the AVF volcanoes, the tephra dispersed
661 by single eruption is not thought to cover the entire field for any single event
662 (Kermode 1992). Therefore, the distribution and thickness of tephra deposits
663 can be indicative of the region within the field where the source centre is located.
664 For example, tephra deposits that are only found in the northern maar sites
665 (Onepoto, Pupuke, Orakei, Glover Park) are inferred to indicate sources in the
666 north or central AVF (based on the dominant wind direction, discussed below).
667 Conversely a deposit only found in the southern maar site (Pukaki) is suggestive
668 of sources in the south of the field. Tephra deposits found in both northern and
669 southern maar sites are likely to have been derived from the central part of the
670 field, and/or reflect an eruption large enough to widely disperse tephra from any
671 source site within the field.
672 Wind direction is also considered, where possible, when making source
673 correlations, because it has a controlling influence on tephra dispersal. For the
674 Auckland region, evidence of prevailing past wind directions can be inferred
675 from the morphology of the volcanic centres, for example, asymmetric tuff rings
676 or scoria cones (e.g. Motukorea, Hayward et al. 2011). Such morphological
677 indications are not however definitive for the majority of centres because there
678 has often been post-depositional erosion, so present cone morphology is not
679 seen as a definitive wind-direction indicator for an individual eruption. The
680 dominant prehistoric wind patterns (westerly/south-westerly) are, however,
681 still the dominant patterns for today (Houghton et al. 2006). This wind direction
682 generally has resulted in more frequent tephra deposition in the northeast and
683 east of the field, confirmed by the high number of deposits found within the
684 Orakei Basin core, situated north-east of most centres (**Fig. 1**). Tephra deposits

685 are therefore more readily traced back to sources to the west and southwest.
686 Conversely, centres found to the east or north east of the maar sites (e.g. Pigeon
687 Mt., Hampton Park, Otara, Green Mt., and Styaks Swamp; **Fig. 1**) are less likely to
688 be represented in the maar-lake tephra record.

689 Hopkins et al. (2015) detailed twenty-eight tephra horizons within six cores.
690 Eleven of the horizons are cross-correlated between cores, linking two or more
691 deposits, and seventeen tephra horizons are single deposits found only within
692 single cores. We here have reduced the number of single horizons to sixteen, and
693 increased the number of cross-correlated horizons to twelve based on the
694 correlation of horizons AVF16/AVF13 as previously discussed.

695 For correlation purposes, we assess each tephra horizon individually; all
696 potential sources are accounted for and discussed, without bias from any other
697 correlations made (see **Supplementary Material**). A 'confidence value' is
698 assigned for each correlation based on the number of supporting criteria that are
699 satisfied (i.e. age, geochemistry, scale and location). In general, if all four criteria
700 are satisfied a confidence level of 1 is given, when three are satisfied a
701 confidence level of 2 is given, and if only two are satisfied a confidence level of 3
702 is given (detailed in **Table 4**). Each of these criteria is variably weighted in
703 importance with age ≥ geochemistry >> locality ≥ eruptive scale. In some cases
704 the confidence level is skewed to reflect this weighting of criteria, and this skew
705 is detailed for each individual case in the supplementary material.

706 Discussion of the correlation of all 28 horizons to their proposed source can
707 be found in the **supplementary material**, with an example of the discussion
708 outlined below for a single representative tephra horizon (AVF5). For each of the
709 horizons the proposed source centres are given in **Table 4** along with

alternatives that were considered. Of the twenty-eight horizons, eight have been given a correlation with confidence level of 1, eleven have been given a confidence level of 2, and seven have been given a confidence level of 3, with two horizons remaining uncorrelated (**Table 4**).

Example of multi-criteria discussion for a level 3 correlation

AVF5 is a thick (110 mm) geochemically homogeneous deposit found only in the Orakei Basin core at a depth of 57.44 m. The bulk tephra sample contains coarse glass shards (>250 μm) and abundant country-rock lithic grains. The source is thus inferred to be relatively close to Orakei Basin in the north of the field. Its modelled sedimentation rate age is of 34.2 ± 0.9 ka (**Table 2**.). Mt. Cambria is the only candidate with the appropriate age and location, however it is one of the smallest centres in the field with an estimated tephra volume (ETV) of 0.44 $x10^6$ m^3 (**Table 2**). It is located ca. 5 km away from Orakei Basin, and therefore, it is highly improbable that it would have produced a 110 mm thick tephra deposit within the basin. Several other centres have appropriate locations and eruption scales, but are older than 35 ka ($^{40}Ar/^{39}Ar$ age ranges [95 % confidence] from Leonard et al. 2017): Mt. Hobson (45.3-68.5 ka), Mt. St John (71.9-78.7 ka), Mt. Victoria (AVF4) (42.8-72.4 ka), and North Head (72.3-102.7 ka), or conversely, too young; Little Rangitoto (AVF14) (16.3-25.1 ka), Taylors Hill (AVF10) (24.2-30.6 ka), and Panmure Basin (AVF13) (>17.5 ka). Of these centres only Mt. Victoria and Mt. Hobson have a similar (overlapping within error) geochemical signature to the tephra-derived glass within the AVF5 horizon. Mt. Victoria has an ETV of 3.9 $x10^6$ m^3 and is located 4.7 km to the northwest of Orakei. In comparison Mt. Hobson has an ETV of 1.8 $x10^6$ m^3 and is

734 2.5 km downwind to the south west of Orakei basin. Based on this, Mt. Hobson is
735 more likely than Mt. Victoria to have produced a thick deposit with large shards
736 in Orakei Basin. The $^{40}Ar/^{39}Ar$ age for Mt. Hobson (44.9-66.9 ka) is older than the
737 modelled AVF5 tephra horizon age, but the only morphostratigraphic constraint
738 is that **Mt. Hobson** is older than Three Kings (consistent with this correlation).
739 We therefore discount the age constraints, which are separated by 9.8 kyr
740 beyond error bounds. This correlation is predominantly based on the locality
741 and scale of eruption and the deposit, with inconclusive geochemistry; it is
742 therefore given a confidence level of 3.
743

744 ***Tephra dispersal in the AVF***

745 Using confident correlations (level 1 and 2 only, which depend primarily on
746 age and geochemistry) of tephra horizons from cores to their source centres,
747 inferences can be made about the dispersal distances and thickness of the
748 deposits from the AVF eruptions. **Table 5** outlines the distance (from source to
749 depositional core site), thickness (primary horizon thickness identified by
750 Hopkins et al. 2015), and (where applicable) the estimated shard sizes (based on
751 grain sieving during glass shard extraction) for each of the centres that have
752 been assigned a correlation with confidence level 1 or 2. There are no
753 contemporaneous subaerial deposits in Auckland (cf. Hopkins et al. 2015), and
754 the recorded thicknesses are here considered to be minima due to potential
755 post-depositional compaction and erosion (Óladóttir et al. 2012).

756 For all correlations with a confidence level of 1, the maximum dispersal is
757 of 13.5 km, for the Three Kings eruption recorded in Pupuke maar in a deposit 2

758 mm thick with shards of 50-100 μm. For both confidence level 1 and 2
759 correlations, the thickest deposits (≥100 mm) are all found within 6 km from
760 source, with a sharp decrease in deposit thickness (all <80 mm) at distances >6
761 km (**Fig. 10A**). The maximum tephra thickness recorded in the cores is 510 mm;
762 the tephra is from the One Tree Hill eruption in Orakei Basin, 4.6 km from the
763 core site, suggesting that for a relatively large eruption (DRE^{tot}= 0.26 km^3
764 Kereszturi et al. 2013) tephra deposits can be >500 mm thick at distances of >4
765 km. The correlation results also show that shard size decreases with distance
766 from source (**Fig. 10B**), with 60% of deposits <6 km from source having shards
767 >200 μm, which reduces to 45% of deposits 6-12 km away and 0% >12 km from
768 source. These findings are particularly applicable as inputs for tephra dispersal
769 model simulations, evacuation and 'clean-up' forecasting, planning, and
770 management (e.g. Tomsen et al. 2014; Wilson et al. 2014; Hayes et al. 2015).
771 Tephra horizon AVF12 correlates to Mt. Eden (**Fig. 1**), and is one of the
772 most widely dispersed (and thus best preserved) tephra horizons; >10 mm thick
773 in both Pupuke and Pukaki cores, which are 11 km and 12 km from source
774 respectively. The Mt. Eden event also correlates with some of the thickest tephra
775 deposits in the cores; 410 mm in Orakei (4.5 km from source), and 460 mm in
776 Hopua (6 km from source). **Figure 11A** shows the decrease in tephra thickness
777 away from source, coupled with the decrease in tephra shard size. Mt. Eden is
778 also used as an example to show how the core-to-core and core-to-source centre
779 correlations can be used to build isopach maps for the dispersal pattern of the
780 eruption (**Fig. 11B**). The impact of the prevailing westerly winds (Hayward et al.
781 2011) is considered and therefore produces an inferred elliptical tephra
782 dispersal footprint. With a calculated total DRE volume of 0.086 km^3, the

783 eruption of Mt. Eden was one of the largest in the AVF, and therefore illustrates
784 the impacts of a more extreme tephra dispersal event from a larger scale
785 eruption.

786 Smaller eruptions produce more-restricted tephra dispersal; thirteen of the
787 twenty-nine tephra horizons (45%) are only identified within single cores. Small
788 eruptions can nevertheless result in near-source tephra horizons of substantial
789 thickness. For example AVF10, now correlated to the eruption of Taylors Hill
790 (DRE volume of 0.0051 km^3), is restricted to the north of the field with cross-
791 correlated deposits found in Orakei Basin (407 mm at ca. 5 km away), Onepoto
792 (15 mm at ca. 12 km away) and Pupuke (3 mm at ca. 13 km away).

793 Deposits are not necessarily found in all maars along a dispersal pathway.
794 For example AVF4 is found in Orakei Basin (41 mm) and Pupuke (15 mm) but is
795 absent in Onepoto, which lies directly between the two. These dispersal patterns
796 are most likely indicative of either discontinuous preservation and/or complex
797 distal fallout (Molloy et al. 2009).

798 **Table 6** lists tephra dispersal information from selected basaltic volcanic
799 fields worldwide together with those for some AVF centres. Monogenetic basaltic
800 eruptions that show comparable total eruptive volumes, dispersal distances and
801 thicknesses to some of the larger AVF centres include Mt. Gambier (Newer
802 Volcanics, Australia) with an estimated DRE^{tot} = 0.20 km^3 (van Otterloo and Cas
803 2013) and measured tephras ≤5 cm thick at 10-12 km distance (Lowe and
804 Palmer 2005). In comparison One Tree Hill (DRE^{tot} = 0.26 km^3) of the AVF has a
805 measured tephra thickness of 6 cm at 10 km from source (**Table 6**). Marcath
806 Volcano (Lunar Crater volcanic field, Nevada, USA) is of a similar eruptive scale
807 to the mid-range AVF volcanoes, with a DRE^{tot} = 0.06 km^3 (Johnson et al. 2014).

Its tephra is 2 cm thick 7 km from vent, comparable to many AVF eruptions of similar scale, e.g. Mt. Wellington and Three Kings (**Table 6**). It is difficult to find global comparisons for the smaller AVF eruptions, but some of the latter show equivalent values to the larger global examples, for example, Orakei Basin, with a DRE^{tot} of 0.0067 km^3 depositing tephra 4 mm thick at 5 km from vent. A number of factors could potentially contribute to the apparent wider dispersal of tephra from the smaller AVF centres, including the high proportion of phreatomagmatic eruptions seen within the field (**Table 2**), the consistent prevailing wind directions, or the more favourable preservation conditions provided by the maar sites.

Eruption age order resolution for the AVF

The correlation of tephra deposits to their source centres, coupled with $^{40}Ar/^{39}Ar$ ages and morphostratigraphy, enables us to construct a relative age model for 48 of the 53 centres, thus allowing us to re-assess the absolute ages for all centres**.** As previously outlined, although the $^{40}Ar/^{39}Ar$ age data (Leonard et al. 2017) provide improved age constraints for many of the AVF centres, the associated errors preclude ordering eruptive events. We reconstruct the relative temporal eruptive history for the AVF by combining; 1) the mean $^{40}Ar/^{39}Ar$ (Cassata et al. 2008; Leonard et al. 2017) and ^{14}C ages (Lindsay et al. 2011; Needham et al. 2011), 2) the modelled sedimentation rate ages assigned based on tephra horizon correlations and, 3) the relative positions based on morphostratigraphic (cf. **Table 3**) or paleomagnetic constraints (Shibuya et al. 1992; Cassidy 2006; Leonard et al. 2017; **Fig. 12**). For five centres there is not

832 enough information to assign absolute or relative ages, and these centres are
833 therefore not included in the following evaluations. **Table 7** and **Figure 13**
834 present a new relative age order and absolute ages for 48 of the AVF centres as
835 defined by this study. A full discussion of the proposed relative and absolute age
836 order can be found in the **supplementary material**.

837 Two previous studies have attempted reconstructions using statistical
838 methods. Bebbington and Cronin (2011) reconstructed the temporal history of
839 the entire field through age simulations based on tephra horizon correlations,
840 stratigraphic constraints, and radiometric ages. Kawabata et al. (2016) made
841 improvements to this statistical approach but focussed solely on correlating the
842 tephra horizons to sources. The input for the original model simulations of
843 Bebbington and Cronin (2011) included deposit thicknesses and age estimates
844 for basaltic tephra within maar cores (from Sandiford et al. 2001; Shane and
845 Hoverd 2002; Molloy et al. 2009), and age estimates for the AVF centres (from
846 Lindsay et al. 2011). In order to improve on Bebbington and Cronin (2011),
847 Kawabata et al. (2016) used newly refined ages for the rhyolitic and andesitic
848 marker horizons from Lowe et al. (2013) as tie points within their
849 reconstruction, and added wind direction and estimated tephra volumes. This
850 improved modelling showed only 3 correlations that were consistent with the
851 previous research, suggesting how easily new data inputs can dramatically
852 impact the outputs of statistical modelling.

853 When we compare our tephra correlations to those outlined by Kawabata
854 et al. (2016; **Table 4** and **Fig. 13**), there are three common correlations; AVF1
855 and Domain, AVF2 and One Tree Hill, and AVF12 and Mt Eden. There are
856 however a large number of discrepancies that we attribute to differences in

857 input data, in most cases linked to differing tephra horizon characteristics and
858 the improved age constraints provided by Leonard et al. (2017).

859 **Figure 14** shows a comparison of our field-wide absolute and relative
860 chronology results to those of Bebbington and Cronin (2011). There is significant
861 scatter around the 1:1 line, indicating the data sets, and thus the relative orders
862 are significantly different (**Fig. 14A**). For example, Bebbington and Cronin
863 (2011) model 21 centres as older, 18 as younger, and 9 in the same positions as
864 our results show. There are, however only a few large discrepancies (>20
865 positions) between the two studies. Little Rangitoto, Motukorea, and Te Pou
866 Hawaiki were all given much older positions (42nd, 35th, 43rd respectively) than
867 those inferred in this study (13th, 12th, 16th respectively), and McLaughlins Mt.,
868 Mt. Mangere and Mangere Lagoon are given much younger positions (4th, 9th, 12th
869 respectively from Bebbington and Cronin, 2011) than those inferred in this study
870 (30th, 33rd, 34th respectively).

871 For absolute age estimates (**Fig. 14B&C**), variation between the data sets is
872 apparently greater than for the relative age estimates. Only twenty centres show
873 offsets of <5 kyr between the modelled ages and our inferred ages, with the
874 remaining 28 showing larger offsets of between 6.1 kyr (Mt Hobson) up to 124
875 kyr (Te Pou Hawaiki). In addition, the modelled absolute ages (from Bebbington
876 and Cronin 2011) cluster around 30 ka, whereas this study infers a broader
877 spread between 20 and 35 ka for the same centres. The Bebbington and Cronin
878 (2011) model is heavily weighted towards tephra horizons in the 30 ka age
879 range, and this may impart a bias on the age constraints of their model's output.
880 For all centres modelled by Bebbington and Cronin (2011) with ages between 45
881 and 75 ka, the ages appear to be younger than inferred in this study (e.g. One

882 Tree Hill, Mt. Albert, and Tank Farm). Conversely, modelled ages for centres
883 older than 75 ka seem to be over estimates (e.g. Little Rangitoto, Orakei Basin
884 and Onepoto). The conflicting results for both relative and absolute age
885 estimates between the two studies (e.g. for Onepoto, Pupuke, and Tank Farm), is
886 likely to reflect differences in the data inputs.
887

888 ***Implications for the spatial, temporal and geochemical evolution of the Auckland***
889 ***Volcanic Field***

890 *Spatial and temporal evolution*

891 The newly estimated ages for 48 of the 53 centres suggest that 18 centres
892 erupted in the first ca. 140 kyr of the AVF's history (190 – ca. 50 ka), with 30
893 erupting from ca. 50 ka to 0.5 ka. By using the rhyolitic marker horizons (RMHs)
894 as definitive age constraints the number of eruptions per 1000 years (erup/kyr)
895 can be calculated: present to Rerewhakaaitu (Rk) (0-17.5 ka) 0.3 erup/kyr; Rk to
896 Okareka (Ok) (17.5–21.5 ka) eruption rate of 1.0 erup/kyr; Ok to
897 Kawakawa/Oruanui (Kk) (21.5–25.4 ka) eruption rate of 1.5 erup/kyr; Kk to
898 Rotoehu (Re) (25.4–52 ka) eruption rate of 0.6 erup/kyr and Re to inception (52-
899 193 ka) eruption rate of 0.13 erup/kyr. These results suggest that in general
900 there was an increase in the eruption frequency through time until ca. 21.5 ka
901 (Okareka RMH; **Table 7**), followed by a decrease since 21.5 ka. Field-repose
902 periods show a wide range from <0.1–13 kyr (**Table 7**), however eruptions are
903 not evenly distributed within this range. Only six centres show field-repose
904 periods of 10-13 kyr, whereas, twenty-three centres erupted after field-repose
905 periods of 1000 years or less (all except four of which are younger than 50 ka),

and eighteen of these twenty-three have field-repose periods of 500 years or less. In general the longer field-repose periods occur at the beginning of the field's history, with all of the six centres with field-repose periods of 10-13 kyrs appearing between 193–86 ka.

The distance between successive eruptions (**Table 7**) varies from <0.5 km to 14 km with two outliers events taking place 21 and 19 km from sites of preceding events. There is spatial but not temporal alignment of some centres for example McLaughlins Hill – Wiri Mt. – Ash Hill (**Fig. 1**); these alignments have previously been attributed to pre-existing crustal fractures and faults (Magill et al. 2005; von Veh and Németh 2009; Kereszturi et al. 2014). In general there is no obvious spatial progression or pattern in location of vents through time.

Previous studies (Bebbington 2013; Le Corvec et al. 2013) have suggested that the location of each centre is independent of that of the previous centre, and for the most part the results presented in this study support this suggestion. When centre location is linked with the temporal evolution, however, a number of centres appear to have erupted very closely in space *and* time. These 'coupled' centres are here defined as having a field-repose period of 1000 years or less and with centres erupting <1 km away from each other. For example Mt. Wellington and Purchas Hill are dated to 10.5 ka and 11 ka respectively and are located ca. 0.5 km apart. The other centres include Rangitoto 1 and 2 (Needham et al. 2011), Styaks Swamp and Green Mt., Mt. Eden and Te Pou Hawaiki, Otara and Hampton Park, and Wiri Mt. and Ash Hill (**Table 7**). It may also be possible to include Onepoto and Tank Farm, Mangere Mt. and Mangere Lagoon, and Domain and Grafton, although the age of one or both volcanoes in each of these pairs is poorly constrained.

Geochemical evolution

The collation of existing, and collection of new, whole rock and tephra-derived glass geochemical data presented here provides the most comprehensive geochemical dataset for the AVF to date (see **Table 1**). These data reveal a more complete view of the field as a whole, and further support the work of McGee et al. (2013, 2015), Hopkins et al. (2016), and McGee and Smith (2016) on the mantle source characteristics and the link between geochemical signatures of the erupted products (e.g. SiO_2 vs. CaO/Al_2O_3 (**Fig. 17A**), or SiO_2 vs. $(La/Yb)_N$ (**Fig. 17B**)) and the eruptive volume for the centres (from Kereszturi et al. 2013). The new field-wide data set produced by this study shows that for SiO_2 vs. CaO/Al_2O_3 the trend in the data is less well defined in comparison to SiO_2 vs. $(La/Yb)_N$ (**Fig 17**). This greater scatter is attributed to the impact of minor amounts of fractional crystallisation on major elements during magma ascent (e.g. Hopkins et al. 2016). The $(La/Yb)_N$ ratio shows a much stronger trend because these two elements are incompatible, thus less effected by fractional crystallisation, and therefore are more reflective of the mantle source signature.

In addition, McGee et al. (2013) highlighted a relationship between the trends observed in trace element multi-plots and eruptive volumes, suggesting that K and Sr anomalies (c.f **Fig. 4**) are also linked to eruptive volume. This conclusion was, however, based on geochemical data for only 10 centres (spanning a wide range in eruptive volumes). The addition of our new data suggests that these relationships may be less clear-cut. For example, the geochemical data for whole-rock samples from Te Pou Hawaiki shows a highly subdued K anomaly, coupled with a large Sr anomaly. This signature was linked by McGee et al. (2013) to centres with large eruptive volumes (e.g. Rangitoto

DRE^{tot} = 0.6 km^3), yet Te Pou Hawaiki has a relatively small estimated volume (DRE^{tot} = 0.028 km^3). Similarly, Mt Cambria has one of the smallest eruptive volumes (DRE^{tot} = 0.00029 km^3), much smaller than Purchas Hill (DRE^{tot} = 0.0017 km^3), yet does not have a more extreme geochemical signature than Purchas Hill (e.g. it lacks a more pronounced K anomaly, or Zr-Hf trough; **Fig. 4**).

If the McGee et al. (2013, 2015) correlations are accepted, then a number of the newly analysed centres exhibit geochemical signatures that are suggestive of larger magma batches than fit their inferred eruptive volumes (e.g. Te Pou Hawaiki; **Fig. 15**). There are three possible explanations for these discrepancies: 1) volume estimates are inaccurate, 2) magma volume is 'lost' on ascent, or 3) the mantle source is heterogeneous.

Volume estimates by Kereszturi et al. (2013) are considered more reliable than those of Allen and Smith (1994), but the same relationships are seen with either data set (**Fig. 15**). Distal tephra is not accounted for in either model, potentially leading to volume underestimates (Kereszturi *pers. comm*.). This underestimate is not, however, enough to account for the observed discrepancies between the geochemical signatures and the erupted volumes. It is possible that there is a loss of magma during ascent, due to either or both of 1) fractional crystallisation of ascending melt, or 2) trapping of magma within the crust as an intrusion. Losses through fractional crystallisation are supported by the less well-defined relationship between the major elements and the erupted volumes as discussed previously. However, because many of the AVF lavas have a very primitive geochemical signature, there is only evidence of very limited fractional crystallisation (e.g. Smith et al. 2008; McGee et al. 2013; Hopkins et al. 2016), which is again not enough to account for the discrepancies. It is therefore most

likely that a heterogeneous mantle source, coupled with minor amounts of fractional crystallisation and retention of magma in the crust, may affect the final proportion of magma that is erupted. When geochemical data are combined with the temporal ordering, there are no obvious patterns identifiable through the history of the field. The lack of systematic change in the geochemical signatures through time suggests that the mantle source is not evolving in any systematic manner. Instead, the magma batches for each eruption are formed through the variable tapping and mixing of these heterogeneous mantle sources.

Conclusions

The collation of whole rock major and trace element data for the AVF has (with a few exceptions) facilitated the development and testing of a method to correlate distal tephra samples to their source volcanic centres. Geochemical correlation between distal tephra-derived glass and the glassy matrix of whole rocks at the source volcano is proved to be reliable. The method produces reasonable results based on major element signatures alone, with correlations strengthened by the use of trace-element signatures. Furthermore, incompatible trace elements and their ratios (particularly versus Yb; e.g. $(Gd/Yb)_N$, $(La/Yb)_N$, $(Zr/Yb)_N$) are representative for individual centres and can therefore be used to geochemically correlate distal basaltic tephra to proximal whole-rock samples in the AVF. Specifically the ratios listed above are proven to be most useful in assigning individual geochemical fingerprints because they are highlighted to be the most variable across the field, yet the least variable within any given centre, and the least affected by fractional crystallisation processes.

1005 This study has demonstrated geochemistry to be an effective tephra
1006 correlation tool, but we stress that geochemical compositions are not always
1007 sufficiently distinct to provide a definitive result. To efficiently correlate tephra
1008 layers to their source centres, a multi-criteria approach is required. For greatest
1009 correlation confidence, this approach combines age data (of both distal tephras
1010 and proximal whole rock deposits) and eruption characteristics (e.g. scale and
1011 locality), to assign the source centre to tephra deposits. Of the twenty eight
1012 basaltic tephra horizons in the AVF maar-lake cores, all but two (newA and
1013 newB) are correlated to a source; eight with a confidence level of 1, eleven with a
1014 confidence level of 2, and seven with a confidence level of 3.

1015 The correlations with confidence levels of 1 and 2 are used to determine
1016 tephra dispersal and thickness (e.g. footprint) from the AVF eruptions. The
1017 maximum tephra dispersal distance is 13.5 km with a primary deposit thickness
1018 within the core of 2 mm, and for all primary core deposits with a thickness >100
1019 mm the source is <6 km away. In a number of cases the deposits are restricted to
1020 sites in close proximity to the source centre, suggesting that in the event of a
1021 future small-scale eruption, damaging thicknesses of tephra will not inundate the
1022 entire Auckland area.

1023 Our correlations also provide a clearer picture of the temporal evolution of
1024 the AVF. Using the stratigraphic relationships of the tephra horizons within the
1025 cores and their association with the rhyolitic marker horizons, the absolute age
1026 order of the centres can be resolved. Because of the errors associated with dating
1027 techniques ($^{40}Ar/^{39}Ar$ and ^{14}C) a relative sequencing of the AVF centres was
1028 previously not possible. Using our new method we provide high-confidence
1029 relative and absolute eruption age estimates for 48 centres, leaving only five

centres with uncertain ages (Pukaki, Pukewairiki, Boggust Park, Cemetery Hill and Puhinui Craters). Our reconstruction of the relative ages of the centres also allows the temporal, spatial, and geochemical evolution of the AVF to be assessed, confirming that there is no simple temporal pattern in the spatial and geochemical evolution of the field.

Acknowledgements

JLH is funded by the DEVORA (DEtermining VOlcanic Risk in Auckland) project, led by Jan Lindsay and Graham Leonard. JLH would like to thank Elaine Smid and Shaun Eaves for field assistance, and David Lowe, Monica Handler and Stephen Blake for valuable discussion and advice during the early stages of this manuscript. The authors wish to thank Neville Hudson at the University of Auckland collections for assistance in finding pre-existing samples, and Bruce Hayward for invaluable advice on site locations for new samples.

References

Affleck DK, Cassidy J, Locke CA (2001) Te Pou Hawaiki volcano and pre-volcanic topography in central Auckland: volcanological and hydrogeological implications. NZ J Geol Geophys 44:313-321

Agustín-Flores J, Németh K, Cronin SJ, Lindsay JM, Kereszturi G (2015) Construction of the North Head (Maungauika) tuff cone: a product of Surtseyan volcanism, rare in the Auckland Volcanic Field, New Zealand. Bull Volcanol 77:11

Allan ASR, Baker JA, Carter L, Wysoczanksi RJ (2008) Reconstructing the Quaternary evolution of the world's most active silicic volcanic system: insights from an ~1.65 Ma deep ocean tephra record sourced from the Taupo Volcanic Zone, New Zealand. Quat Sci Rev 27:2341-2360

Allen SR, Smith IEM (1994) Eruption styles and volcanic hazard in the Auckland Volcanic Field, New Zealand. Geosci Rep Shizuoka Univ 20:5-14

Alloway BV, Westgate JA, Pillans, BJ, Pearce NJG, Newnham RM, Byrami, ML, Aarburg SE (2004) Stratigraphy, age and correlation of middle Pleistocene silicic tephras in the Auckland region, New Zealand: a prolific distal record of Taupo Volcanic Zone volcanism. NZ J Geol Geophys 47:447-479

Bebbington MS (2013) Assessing probabilistic forecasts of volcanic eruption onsets. J Volcanol Geotherm Res 252:14-28

Bebbington MS, Cronin SJ (2011) Spatio-temporal hazard estimation in the Auckland Volcanic Field, New Zealand, with a new event-order model. Bull Volcanol 73:55-72

Brand BD, Gravley DM, Clarke AB, Lindsay JM, Bloomberg SH, Agustín-Flores J, Németh K (2014) A combined field and numerical approach to understanding

dilute pyroclastic density current dynamics and hazard potential: Auckland Volcanic Field, New Zealand. J Volcanol Geotherm Res 276:215-232

Briggs RM, Okada T, Itaya T, Shibuya H, Smith IEM (1994) K-Ar ages, paleomagnetism, and geochemistry of South Auckland volcanic field, North Island, New Zealand. NZ J Geol Geophys 37:143-153

Bryner V (1991) Motukorea: the evolution of an eruption centre in the Auckland Volcanic Field. MSc thesis, University of Auckland, New Zealand.

Cassata WS, Singer BS, Cassidy J (2008) Laschamp and Mono Lake geomagnetic excursions recorded in New Zealand. Earth Planet Sci Lett 268:76-88

Cassidy J (2006) Geomagnetic excursion captured by multiple volcanoes in a monogenetic field. Geophys Res Lett 33:L21310

Charlier BLA, Peate DW, Wilson CJN, Lowestern JB, Storey M, Brown SJA (2003) Crystallisation ages in coeval silicic magma bodies: ^{238}U-^{230Th} disequilibrium evidence from the Rotoiti and Earthquake Flat eruption deposits, Taupo Volcanic Zone, New Zealand. Earth Planet Sci Lett 206:441-457

Cook C, Briggs RM, Smith IEM, Maas R (2005) Petrology and geochemistry of intraplate basalts in the South Auckland volcanic field, New Zealand: Evidence for two coeval magma suites from distinct sources. J Petrol 46:473-503

Danišík M, Shane P, Schmitt AK, Hogg A, Santos GM, Storm S, Evans NJ, Fifield, LK, Lindsay JM (2012) Re-anchoring the late Pleistocene tephrochronology of New Zealand based on concordant radiocarbon ages and combined $^{238}U/^{230}Th$ disequilibrium and (U-Th)/He zircon ages. Earth Planet Sci Lett 349-350:240-250

1107 Davies SM, Turney CSM, Lowe JJ (2001) Identification and significance of a
1108 visible , basalt-rich Vedde Ash layer in a Late-glacial sequence on the Isle of Skye,
1109 Inner Hebrides, Scotland. J Quat Sci 16:99-104
1110
1111 Dunbar NW, Kurbatov AV (2011) Terphrochronology of the Siple Dome ice core,
1112 West Antarctica: correlations and sources. Quat Sci Rev 30:1602-1614
1113
1114 Eade J (2009) Petrology and correlation of lava flows from the central part of the
1115 Auckland Volcanic Field. MSc thesis, University of Auckland, New Zealand.
1116
1117 Fleck RJ, Hagstrum JT, Calvert AT, Evarts RC, Conrey RM (2014) $^{40}Ar/^{39}Ar$
1118 geochronology, paleomagnetism, and evolution of the Boring volcanic field,
1119 Oregon and Washington, USA. Geosphere 10:1483-1314
1120
1121 Flude S, Storey M (2016) $^{40}Ar/^{39}Ar$ age of the Rotoiti Breccia and Rotoehu Ash,
1122 Okataina Volcanic Complex, New Zealand, and identification of heterogeneously
1123 distributed excess ^{40}Ar in supercooled crystals. Quat Geochronol 33:13-23
1124
1125 Franklin JT (1999) Geology of the Orakei Basin area. MSc thesis, University of
1126 Auckland, New Zealand.
1127
1128 Hayes JL, Wilson TM, Magill C (2015) Tephra fall clean-up in urban
1129 environments. J Volcanol Geotherm Res 304:237-252
1130
1131 Hayward BW (2008) Ash Hill Volcano, Wiri. Geocene, Geoscience Society of New
1132 Zealand, 3:8-9
1133
1134 Hayward BW, Hopkins, JL, Smid, ER (2016) Mangere Lagoon predated Mangere
1135 Mt. Geocene, Geoscience Society of New Zealand, 14:4-5
1136
1137 Hayward BW, Murdoch G, Maitland G (2011) Volcanoes of Auckland, The
1138 Essential Guide. Auckland University Press, Auckland, New Zealand.
1139

1140 Heming RF, Barnet PR (1986) The petrology and petrochemistry of the Auckland
1141 volcanic field. In: Smith IEM (Ed), Late Cenozoic Volcanism in New Zealand. Roy
1142 Soc NZ Bull 23:64-75
1143
1144 Hill BE, Connor CB, Jarzemba MS, La Femina PC, Navarro M, Strauch W (1998)
1145 1995 Eruptions of Cerra Negro Volcano, Nicaragua, and risk assessment for
1146 future eruptions Geol Soc Am Bull 110:1231-1241
1147
1148 Hookway M (2000) The geochemistry of Rangitoto. MSc thesis, University of
1149 Auckland, New Zealand
1150
1151 Hopkins JL, Millet, M-A, Timm C, Wilson CJN, Leonard GS, Palin JM, Neil H (2015)
1152 Tools and techniques for developing tephra stratigraphies in lake cores: a case
1153 study from the Auckland Volcanic Field, New Zealand. Quat Sci Rev 123:58-75.
1154
1155 Hopkins JL, Timm C, Millet M-A, Poirier A, Wilson CJN, Leonard GS (2016) Os
1156 isotopic constraints on crustal contamination in Auckland Volcanic Field basalts,
1157 New Zealand. Chem Geol 439:83-97
1158
1159 Houghton BF, Bonadonna C, Gregg CE, Johnston DM, Cousins WJ, Cole JW, Del
1160 Carlo P (2006) Proximal tephra hazards: recent eruptions studies applied to
1161 volcanic risk in the Auckland Volcanic Field, New Zealand. J Volcanol Geotherm
1162 Res 155:138-149
1163
1164 Hoverd JL, Shane PA, Smith IEM, Smith VC, Wilson CJN (2005) Towards an
1165 improved understanding of local and distal volcanic stratigraphy in Auckland:
1166 stratigraphy of a long core from Glover Park (St Helier's Volcano) in Auckland.
1167 Institute of Geological & Nuclear Sciences Science Report 2005/31:45p
1168
1169 Huang Y, Hawkesworth C, van Calsteren P, Smith I, Black P (1997) Melt
1170 generation models for the Auckland volcanic field, New Zealand: constraints
1171 from U-Th isotopes. Earth Planet Sci Lett 149:67-84
1172

1173 Johnson PJ, Valentine GA, Cortés JA, Tadini A (2014) Basaltic tephra from
1174 monogenetic Marcath Volcano, central Nevada. J Volcanol Geotherm Res 281:27-
1175 33
1176
1177 Kawabata E, Cronin S, Bebbington M, Moufti M, El-Masry N, Wang T (2015)
1178 Identifying multiple eruption phases from a compound tephra blanket: an
1179 example of the AD1256 Al-Madinah eruption, Saudi Arabia. Bull Volcanol 77:6
1180
1181 Kawabata E, Bebbington MS, Cronin SJ, Wang T (2016) Optimal likelihood-based
1182 matching of volcanic sources and deposits. J Volcanol Geotherm Res 323:194-
1183 208
1184
1185 Kereszturi G, Németh K, Cronin SJ, Agustín-Flores J, Smith IEM, Lindsay J (2013)
1186 A model for calculating eruptive volumes for monogenetic volcanoes –
1187 Implication for the Quaternary Auckland Volcanic Field, New Zealand. J Volcanol
1188 Geotherm Res 266:16-33
1189
1190 Kereszturi G, Németh K, Cronin SJ, Procter J, Agustín-Flores J (2014) Influences
1191 on the variability of eruption sequences and style transitions in the Auckland
1192 Volcanic Field, New Zealand. J Volcanol Geotherm Res 286:101-115
1193
1194 Kermode LO (1992) Geology of the Auckland urban area. Scale 1:50,000.
1195 Institute of Geological and Nuclear Sciences geological map 2. Institute of
1196 Geological and Nuclear Sciences Ltd, Lower Hutt, New Zealand
1197
1198 Larsson W (1937) Vulkanische asche vom ausbruch des Chilenischen vulkans
1199 Quizapú (1932) in Argentina gesammelt. Bulletin Geological Institution of
1200 Uppsala 26:27-52.
1201
1202 Le Corvec N, Bebbington MS, Lindsay JM, McGee LE (2013) Age, distance and
1203 geochemical evolution within a monogenetic volcanic field: Analysing patterns in
1204 the Auckland Volcanic Field eruption sequence. Geochem Geophys Geosyst
1205 14:3648-3665
1206

LeMaitre RW (2002) Igneous Rocks: Classification and Glossary of Terms. 2nd Edition, Cambridge University Press, Cambridge, UK, pp236.

Leonard GS, Calvert AT, Hopkins JL, Wilson CJN, Smid E, Lindsay J, Champion D (2017) High precision ^{40}Ar-^{39}Ar dating of late Quaternary basalts from Auckland Volcanic Field, New Zealand, with implications for eruption rates and paleomagnetic correlations. Earth Planet Sci Lett (in press)

Lian OB, Shane P (2000) Optical dating of paleosols bracketing the widespread Rotoehu tephra North Island, New Zealand. . Quat Sci Rev 19:1649-1662

Lindsay JM, Leonard GS, Smid ER, Hayward BW (2011) Age of the Auckland Volcanic Field: a review of existing data. NZ J Geol Geophys 54:379-401

Lirer L, Pescatore T, Booth B, Walker GPL (1973) Two plinian pumice-fall deposits from Somma-Vesuvius, Italy. Geol. Soc. Am. Bull. 84:759-772

Lowe DJ (2011) Tephrochronology and its application: a review. Quat Geochronol 6:107-153

Lowe DJ, Hogg AG (1995) Age of the Rotoehu Ash. NZ J Geol Geophys 38:399-402

Lowe DJ, Palmer DJ (2005) Andisols of New Zealand and Australia. J Integr Field Sci 2:39-65

Lowe DJ, Alloway BV (2015) Tephrochronology. *In* Rink WJ, Thompson JW (Eds) Encyclopedia of Scientific Dating methods. Springer, Dordecht 733-799.

Lowe DJ, Blaauw M, Hogg AG, Newham RM (2013) Ages of 24 widespread tephras erupted since 30,000 years ago in New Zealand, with re-evaluation of the timing and palaeoclimatic implications of the Late Glacial cool episode recorded in the Kaipo bog. Quat Sci Rev 74:170-194

1240 Magill CR, McAneney KJ, Smith IEM (2005). Probabilistic assessment of vent
1241 locations for the next Auckland Volcanic Field event. Math Geol 37:227-242.
1242
1243 McDonough WF, Sun S-s (1995) The composition of the Earth. Chem Geol
1244 120:223-253
1245
1246 McGee LE (2012) Melting processes in small basaltic systems: the Auckland
1247 Volcanic Field, New Zealand. Ph.D. thesis, University of Auckland, New Zealand.
1248
1249 McGee LE, Smith IEM (2016) Interpreting chemical compositions of small scale
1250 basaltic systems: A review. J Volcanol Geotherm Res 325:45-60
1251
1252 McGee LE, Beier C, Smith IEM, Turner S (2011) Dynamics of melting beneath a
1253 small-scale basaltic system: a U-Th-Ra study from Rangitoto volcano, Auckland
1254 Volcanic Field, New Zealand. Contrib Mineral Petr 162:547-563
1255
1256 McGee LE, Millet M-A, Smith IEM, Németh K, Lindsay JM (2012) The inception
1257 and progression of melting in a monogenetic eruption: Motukorea Volcano, the
1258 Auckland Volcanic Field, New Zealand. Lithos 156:360-374
1259
1260 McGee LE, Smith IEM, Millet M-A, Handley H, Lindsay JM (2013) Asthenospheric
1261 control of melting processes in a monogenetic basaltic system: a case study of
1262 the Auckland Volcanic Field, New Zealand. J Petrol 54:2125-2153
1263
1264 McGee LE, Millet M-A, Beier C, Smith IEM, Lindsay JM (2015) Mantle
1265 heterogeneity controls on small-volume basaltic eruption characteristics.
1266 Geology 43:551-554
1267
1268 McKenzie D, O'Nions RK (1991) Partial melt distributions from inversion of rare
1269 earth element concentrations. J Petrol 32:1021-1091
1270
1271 Miller CA (1996) Geophysical and geochemical characteristics of the Auckland
1272 Volcanic Field. MSc thesis, University of Auckland, New Zealand.

Molloy CM (2008) Tephrostratigraphy of the Auckland maar craters. MSc thesis, University of Auckland, New Zealand.

Molloy C, Shane P, Augustinus P (2009) Eruption recurrence rates in a basaltic volcanic field based on tephra layers in maar sediments: implications for hazards in the Auckland volcanic field. Geol Soc Am Bull 121:1666-1677

Needham AJ, Lindsay JM, Smith IEM, Augustinus P, Shane PA (2011) Sequential eruption of alkaline and subalkaline magmas from a small monogenetic volcano in the Auckland Volcanic Field, New Zealand. J Volcanol Geotherm Res 201:126-142

Newnham RM, Lowe DJ, Giles T, Alloway BV (2007) Vegetation and climate of Auckland, New Zealand, since ca. 32000 cal. yr ago: support for an extended LGM. J Quat Sci 22:517-534

Óladóttir BA, Larsen G, Sigmarsson O (2012) Deciphering eruption history and magmatic processes from tephra in Iceland. Jökull 62:21-38

Ort MH, Elson MD, Anderson KC, Duffield WA, Hooten JA, Champion DE, Waring G (2008) Effects of scoria-cone eruptions upon nearby human communities. Geol Soc Am Bull 120:476-486

Paton C, Hellstrom J, Paul B, Woodhead J, Hergt J (2011) Iolite, freeware for the visualisation and processing of mass spectrometric data. J Anal Atom Spectrom 26:2508-2518

Pearce NJ, Alloway BV, Westgate JA (2008) Mid-Pleistocene silicic tephra beds in the Auckland region, New Zealand: their correlation and origins based on the trace element analyses of single glass shards. Quaternary International 178:16-43

1306 Pyle DM (1989) The thickness, volume and grain size of tephra fall deposits. Bull
1307 Volcanol 51:1-15
1308
1309 Pyne O'Donnell S (2011) The taphonomy of Last Glacial-Interglacial Transition
1310 (LGIT) distal volcanic ash in small Scottish lakes. Boreas 40:131-145
1311
1312 Ramsey MH, Potts PJ, Webb PC, Watkins P, Watson JS, Coles BJ (1995) An
1313 objective assessment of analytical method precision: comparison of ICP-AES and
1314 XRF for the analysis of silicate rocks. Chem Geol 124:1-19
1315
1316 Reiners PW (1998) Reactive melt transport in the mantle and geochemical
1317 signatures of mantle-derived magmas. J Petrol 39:1039-1061
1318
1319 Robinson JA, Wood BJ (1998) The depth of the spinel to garnet transition at the
1320 peridotite solidus. Earth Planet Sci Lett 164:277-284
1321
1322 Sandiford A, Alloway B, Shane P (2001) A 28,000-6600 cal yr record of local and
1323 distal volcanism preserved in a paleolake, Auckland, New Zealand. NZ J Geol
1324 Geophys 44:323-336
1325
1326 Sandiford A, Horrocks M, Newnham R, Ogden J, Alloway B (2002) Environmental
1327 change during the last glacial maximum (c. 25000 – c. 16500 years BP) at Mt
1328 Richmond, Auckland Isthmus, New Zealand. J Roy Soc New Zeal 32:155-167
1329
1330 Shane P (2005) Towards a comprehensive distal andesitic tephrostratigraphic
1331 framework for New Zealand based on eruptions from Egmont Volcano. J Quat Sci
1332 20:45-57
1333
1334 Shane P, Hoverd J (2002) Distal record of multi-sourced tephra in Onepoto Basin,
1335 Auckland, New Zealand: implications for volcanic chronology, frequency and
1336 hazards. Bull Volcanol 64:441-454
1337

1338 Shane P, Smith IEM (2000) Geochemical fingerprinting of basaltic tephra
1339 deposits in the Auckland Volcanic Field. NZ J Geol Geophys 43:569-577
1340
1341 Shane P, Gehrels M, Zawalna-Geer A, Augustinus P, Lindsay J, Chaillou I (2013)
1342 Longevity of a small shield volcano revealed by crypto-tephra studies (Rangitoto
1343 volcano, New Zealand): Change in eruptive behaviour of a basaltic field. J
1344 Volcanol Geotherm Res 257:174-183
1345
1346 Shibuya H, Cassidy J, Smith IEM, Itaya T (1992) A geomagnetic excursion in the
1347 Brunhes epoch recorded in New Zealand basalts. Earth Planet Sc Lett 111:41–48
1348
1349 Smith IEM, Blake S, Wilson CJN, Houghton BF (2008) Deep-seated fractionation
1350 during the rise of a small-volume basalt magma batch: Crater Hill, Auckland, New
1351 Zealand. Contrib Mineral Petrol 155:511-527
1352
1353 Spargo SRW (2007) The Pupuke volcanic centre: polygenetic magmas in a
1354 monogenetic field. MSc thesis, University of Auckland, New Zealand
1355
1356 Tomsen E, Lindsay JM, Gahegan M, Wilson TM, Blake DM (2014) Evacuation
1357 planning in the Auckland Volcanic Field, New Zealand: a spatio-temporal
1358 approach for emergency management and transportation network decisions.
1359 Journal of Applied Volcanology 3:6
1360
1361 Ukstins Peate I, Kent AJR, Baker JA, Menzies MA (2008) Extreme geochemical
1362 heterogeneity in Afro-Arabian Oligocene tephras: preserving fractional
1363 crystallisation and mafic recharge processes in silicic magma chambers. Lithos
1364 102:260-278
1365
1366 Valentine GA, Krier D, Perry FV, Heiken G (2008) Eruptive and geomorphic
1367 processes at the Lathrop Wells scoria cone volcano. J Volcanol Geotherm Res
1368 161:57-80
1369

van Otterloo J, Cas RAF (2013) Reconstructing the eruption magnitude and energy budgets for the pre-historic eruption of the monogenetic ~5 ka Mt. Gambier Volcanic Complex, south-eastern Australia. Bull Volcanol 75:769

von Veh MW, Németh K (2009) An assessment of the alignments of vents based on geostatistical analysis in the Auckland Volcanic Field, New Zealand. Géomorphologie: relief, processus, environment 15:175-186.

Wilson CJN, Rhoades DA, Lanphere MO, Calvert AT, Houghton BF, Weaver SD, Cole JW (2007) A multi-approach radiometric age estimate for the Rotoiti and Earthquake Flat eruptions, New Zealand, with implications for the MIS 4/3 boundary. Quat Sci Rev 26:1861-1870

Wilson G, Wilson TM, Deligne NI, Cole JW (2014) Volcanic hazard impacts to critical infrastructure: a review. J Volcanol Geotherm Res 286:148-182

Zawalna-Geer A, Lindsay JM, Davies S, Augustinus P, Davies S (2016) Extracting a primary Holocene cryptotephra record from Pupuke maar sediments, Auckland, New Zealand. J Quat Sci 31:442-457

Figure Captions

Figure 1. (A) Map of the Auckland Volcanic Field and its eruptive centres (from Hayward et al. 2011). The locations of maar craters from which cores documented here were collected are highlighted by red symbols and red font: Pupuke, Onepoto, Glover Park, Orakei, Hopua and Pukaki. Although the Glover Park core is from St Heliers volcano, to avoid confusion here the core location will continue to be called Glover Park. (B) General location of the AVF within the North Island, New Zealand. Highlighted are other key volcanic centres including the South Auckland Volcanic Field (SAVF), and the key rhyolitic sources from the Taupo Volcanic Zone (TVZ) (Taupo Volcanic Centre (TVC), Okataina Volcanic Centre (OVC)) and andesitic (Tongariro Volcanic Centre (TgVC), Mt. Taranaki (Tk/Eg)) sources of tephra found in Auckland maar crater cores.

Figure 2. Age-depth profiles for rhyolitic marker horizons (RMHs) and basaltic tephra deposits within the cores, and individual sedimentation rate profiles for each core. Abbreviations, errors, and references for the RMHs ages are in **Table 2**. Age envelopes are highlighted in light grey based on the errors associated with the RMH ages. AVF basaltic deposits are plotted as red triangles at the appropriate depth in the core, and horizon Eg36, an andesitic marker horizon from Mt Taranaki, is plotted in green.

Figure 3. Representative major and trace element variation diagrams (in wt%) for AVF volcanic rocks (n=744; data in **supplementary material**). Highlighted are those which show examples of the distinct patterns seen within individual centres, grey symbols show all other data.

Figure 4. Primitive mantle-normalised trace element plots for whole rock (shaded grey) and glass from selected tephra horizons (coloured lines) from a range of cores showing a range of geochemistries and ages (high AVF#s = young, low AVF# = old). Values are normalised to primitive mantle after McDonough and Sun (1995).

Figure 5. Comparison plot for concentrations of major and trace elements for whole rock and glass for the full sample suite (all data in **supplementary material**). (A) MgO vs. SiO_2 indicating an example of elements that do not correlate, and (B) $(Zr/Yb)_N$ vs. $(Gd/Yb)_N$ indicating an example of trace element ratios that do correlate for glass and whole rock samples.

Figure 6. Multi-element plots to show geochemical comparison between glass from a known Mt. Wellington tephra deposit from the Hopua maar core, a simulated glass (matrix-derived glass) made from Mt. Wellington whole rock sample AU62394, and whole rock analyses from Mt Wellington. (A) Glass comparison of MgO vs. Al_2O_3, (B) glass comparison for Gd vs. Zr, (C) example of glass and whole rock concentrations for major elements which are not comparable (MgO vs Al_2O_3), (D) example of glass and whole rock major element concentration that are comparable (CaO vs FeO), (E) example of glass and whole rock trace elements that are comparable (Tm vs. Gd), (F) example of glass and whole rock trace element ratios that are comparable ($(Zr/Yb)_N$ vs. $(Gd/Yvb)_N$). Individual analyses are shown by symbols, field-wide geochemical concentrations of glass are outlined by orange dashed area and field-wide geochemical whole rock concentrations are shown by black dashed area.

Figure 7. Selected whole rock and glass sample concentrations to show the effects of crystal removal. (A) MgO vs. Ni for glass and, (B) whole rock. Both show a high r^2 value suggesting a statistically significant relationship between the two elements. In comparison (C) MgO vs. La for glass and, (D) for whole rock. Both show r^2 values near zero, indicating no statistically significant relationships between the elements.

Figure 8. Graphs showing the variations and comparability of the geochemical signatures observed through the eruptive products of Motukorea volcano (from McGee et al. 2012), coupled with the geochemical signatures for the distal glass composition found within the Orakei Basin core (horizon AVF15). (A) SiO_2 (wt%) vs. Zr (ppm) and (B) $(Zr/Yb)_N$ vs. $(Gd/Yb)_N$ normalised to primitive mantle values (McDonough and Sun 1995). Similar relationships are also seen for $(La/Yb)_N$, $(Ce/Yb)_N$, $(Nb/Yb)_N$, and $(Nd/Yb)_N$) (data from **supplementary material**).

Figure 9. Example plots of geochemical correlations. Glass values are shown in coloured symbols that indicating different cores, whole rock values are shown by coloured triangles for each centre, and the grey field shows the geochemical spread for the entire AVF, both whole rock and glass compositions. (A) Example of a confidence level 1 correlation for the Three Kings centre with tephra layer AVF7, showing selected major element and normalised trace element ratios. (B) Example of an ambiguous geochemical correlation for Crater Hill centre and tephra horizon AVF8 due to limited trace element geochemistry for some centres. (C) Example of centres that are of an appropriate age but show no geochemical correlation to the tephra horizon AVF13.

Figure 10. Data for all correlations with a confidence rating of level 1 or 2 (data in **Table 6**). (A) Horizon thickness vs. distance from source, showing the thinning of deposits increases away from source. Grey shaded area marks <6 km, within which all the deposits >100 mm thick are found. (B) % Shard size vs. distance from source, indicating the fining of away from source.

Figure 11. Example of the correlation of Mt. Eden eruption to tephra deposit AVF12. (A) Graph to show change in deposit thickness away from source, note the extreme decline in thickness after ca. 6 km distance. Also shown on (A) are backscatter electron images of the glassshards from each core site taken on EMPA. All pictures are at the same scale with the bar at the base of the images representing 200 μm. (B) Inferred isopach map of the tephra dispersal from Mt. Eden based on the deposit thicknesses found in the cores. Dispersal is skewed to the east to reflect the westerly winds likely to have been present at the time of eruption (Hayward et al. 2011).

Figure 12. Age range chart for all centres (data from **Table 5.1**). Those in red are $^{40}Ar/^{39}Ar$ (from Leonard et al. 2017 or Cassata et al. 2008) (2 sd error) or ^{14}C ages (from Lindsay et al. 2011). Markers show the mean ages measured by these techniques with lines showing the age ranges measured. Lines in orange have their ages based only on morphostratigraphy, and those in grey have no ages associated with them. Of note is the number of centres which, based on errors, could have erupted at a given time. For example there are 18 potential centres whose age ranges include 50 ka (Mt. Cambria, McLaughlins Hill, Hopua, One Tree Hill, Mt. Victoria, Mt. Hobson, Waitomokia, Onepoto, St Heliers, Tank Farm, Domain, Grafton, Otuataua, Puhinui Craters, Mt. Robertson, Cemetery Hill, Boggust Park, and Pigeon Mt.).

Figure 13. Figure to show the combined age data that allow the centres to be put in order. Core correlations are from Hopkins et al. (2015), AVF horizon correlations from this study, Ar-Ar ages and ranges from Leonard et al. (2017), and morphostratigraphic relationships from Allen and Smith (1994); Affleck et al. (2001); and Hayward et al. (2011). Key rhyolitic marker horizons are shown in colours, and highlight the chronostratigraphic age limits for the basaltic horizons. Age ranges depicted by error bars are not to scale, the ranges are drawn to the associated ages in the cores.

Figure 14. A comparison of relative and absolute age orders for 45 AVF centres from statistical modelled results (Bebbington and Cronin 2011) versus new data from this study. (A) Relative age order, (B) absolute age estimates, and (C) 10-50 ka for absolute age. The 1:1 ratio lines are shown in red on each chart for comparison purposes.

Figure 15. Comparison plots for whole rock geochemistry vs. eruptive volume for all data available from the AVF. Data are plotted versus eruptive volume estimates from both Kereszturi et al. (2013) and Allen and Smith (1994) for comparison. All data are shown in light grey symbols, with mean values for each centre highlighted for pre-existing data in grey triangles, and for new data in red triangles.

Table Captions

Table 1. Catalogue of geochemical whole rock data (pre-existing and additions from this study) available for the AVF, ordered by the number of analyses, including those centres without any current data. After the addition of data in this paper, 44 centres now have 3 or more geochemical data points.

Table 2. Details of all 53 centres in the AVF, their eruption type; the current age estimate and method by which the ages are calculated, the relative age relationships where known including, and the morphological features which give age constraints. Sources are: a. Hayward et al. (2011); b. Allen and Smith (1994); c. Affleck et al. (2001); d. Sandiford et al. (2002); e. Lowe et al. (2013); f. Lindsay et al. (2011); g. Kermode (1992); h. Newnham et al. (2007); i. Agustín-Flores et al. (2015); j. Leonard et al. (2016); k. Hayward et al. (2016); the estimated dense rock equivalent (DRE) volumes for the total, tuff ring and scoria cone from Kereszturi et al. (2013); and the calculated tephra volumes using the equation reported in Kawabata et al. (2015). For the eruption types, (A) phreatomagmatic wet explosive eruption which produces maar craters and tuff rings, (B) dry magmatic eruptions including fire fountaining creating scoria cones, and (C) effusive eruptions resulting in lava flows, and shield building.

Table 3. The ages and associated errors calculated for each basaltic horizon using either, Monte Carlo simulations for those younger than the Maketu RMH, and sedimentation rate calculations for those older than the Maketu RMH (*italicised*)**.** References: a. Needham et al. (2011); b. Lowe et al. (2013); c. Molloy (2008); d. D.J. Lowe *pers comm* (2016); and e. Leonard et al. (2016). AVF24 is split into Rangitoto (Ra)1 and 2 identified and dated (^{14}C in cal. yr. BP) by Needham et al. (2011), *indicates nomenclature from Molloy et al. (2009) for the tephra horizons found in the Pupuke core. The ages for the rhyolitic marker horizons (shaded grey) are outlined in cal. yr. BP. The age of AVF17 is shown in grey text as an outlier, and the position of AVF16 also shown in grey text as out of sequence, both of these are discussed in the text. The age of deposit AVFd in the base of the Onepoto core is taken from the minimum ^{40}Ar/^{39}Ar age estimation for Pupuke centre, see text for details. All errors are reported as 2 s.d., and the 95% confidence limits are also reported.

Table 4. Outline of correlations for individual tephra horizons to their source centre. Average age are calculated by this study (**Table 3**). Proposed centre is given in bold with

certainty value (scale 1-3). Ticks indicate where correlation satisfies the criteria of age (within error of radiometric age), chemistry, scale, and location, '?' indicated where centre ages are unknown. Alternative possible centres are outlined with their certainty value and criteria. See supplimentary material for explaination of ambiguities in the table in relation to rating given.

Table 5. For those deposits with a correlation certainty of 1 or 2, the distance to the deposition site (core) (km), thickness of the deposit within the core (mm) and the average shard size of the tephra (μm) are shown.

Table 6. Comparative global values for tephra dispersal, thickness and total dense rock equivalent (DRE) volume (in km^3; from Kereszturi et al. 2013 to allow global comparisons) for monogenetic basaltic volcanoes. * Cerro Negro is a polygenetic scoria cone, however it has a comparable total volume estimate from the 1995 basaltic eruption, and is therefore deemed applicable for comparison. In bold are examples from this study to allow a direct comparison.

Table 7. Relative order of eruptions with calculated mean ages, time and distance relationship between the n^{th}, n+1 and n+2 centre. References include a. tephra horizon ages from this study; b. ^{14}C from Lindsay et al. 2011; c. Ar-Ar from Leonard et al. 2016 or Cassata et al., 2008 (see **Table 3**); d. morphostratigraphic constraints (references in **Table 3**) and/or paleomagnetic constraints (from Shibuya et al. 1992). Absolute ages evaluated by this study are discussed in detail in the supplimentary material. Note that for centres where morphostratigraphy suggests contemporaneous eruptions (e.g., no material between sucessive volcanic deposits) an arbritrary difference of 500 years is assigned based on a minimum time taken to form soil horizons.

Figure 1

Click here to download Figure Figure 1.png

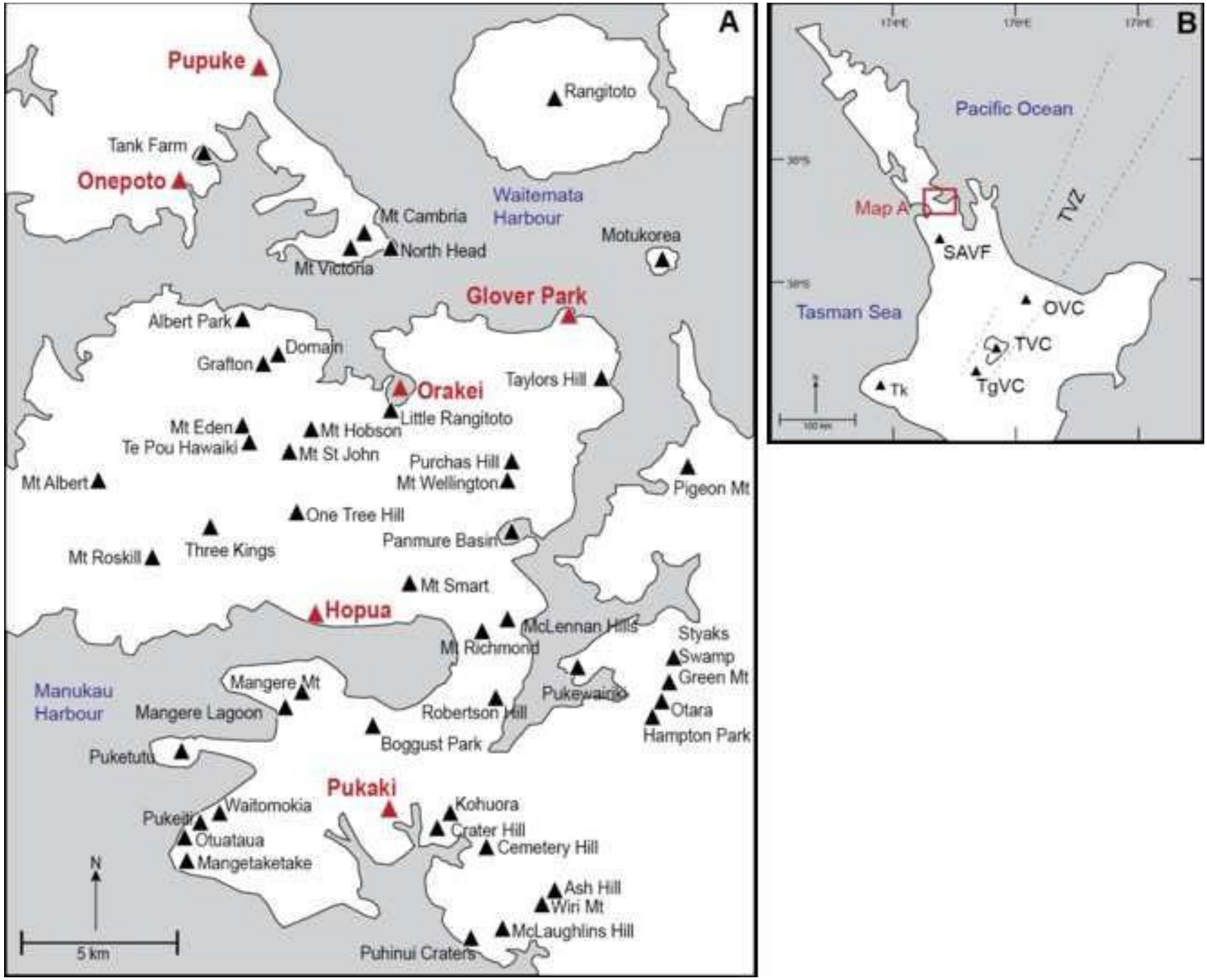

Figure 2

Click here to download Figure Figure 2.png

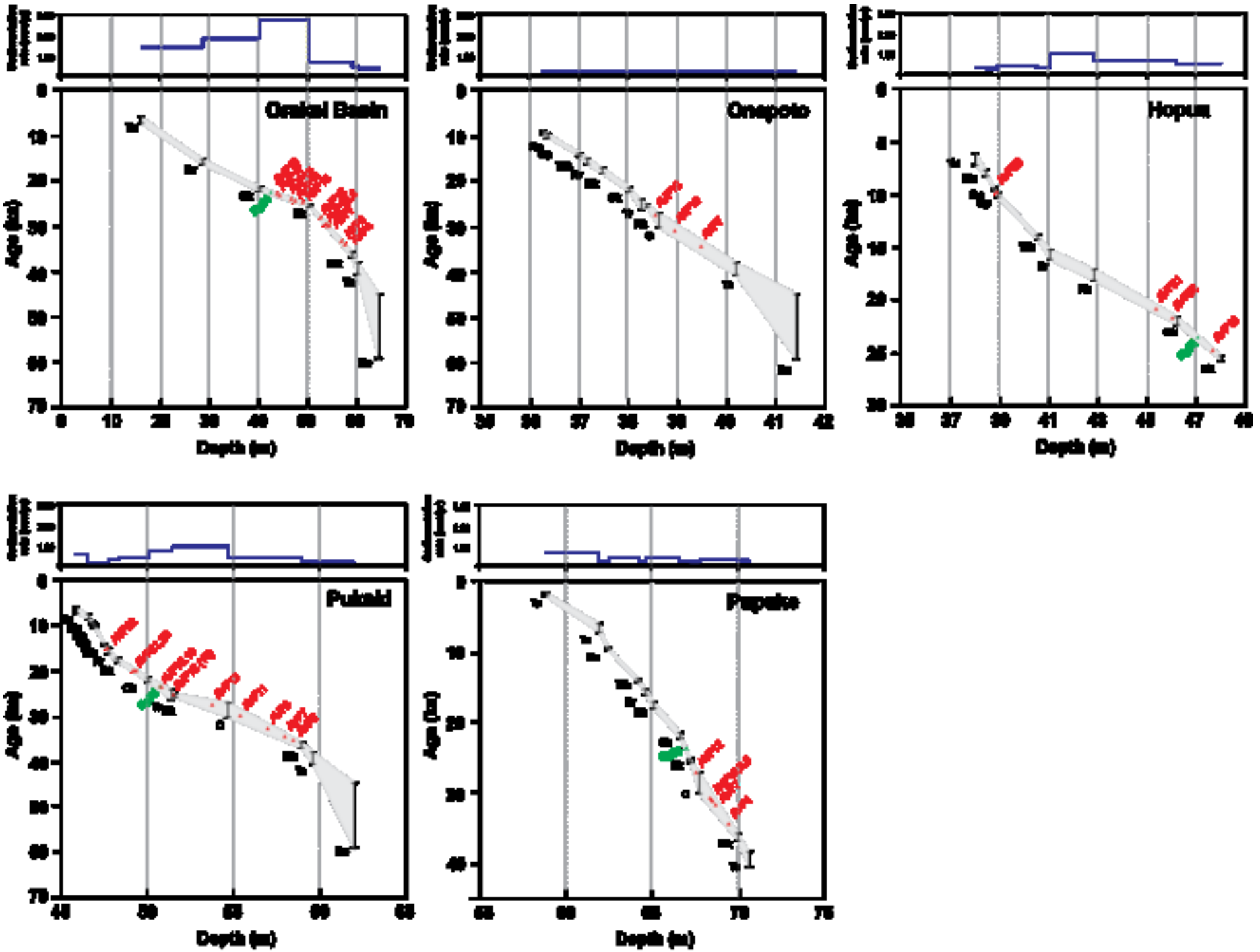

Figure 3

Click here to download Figure Figure 3.png

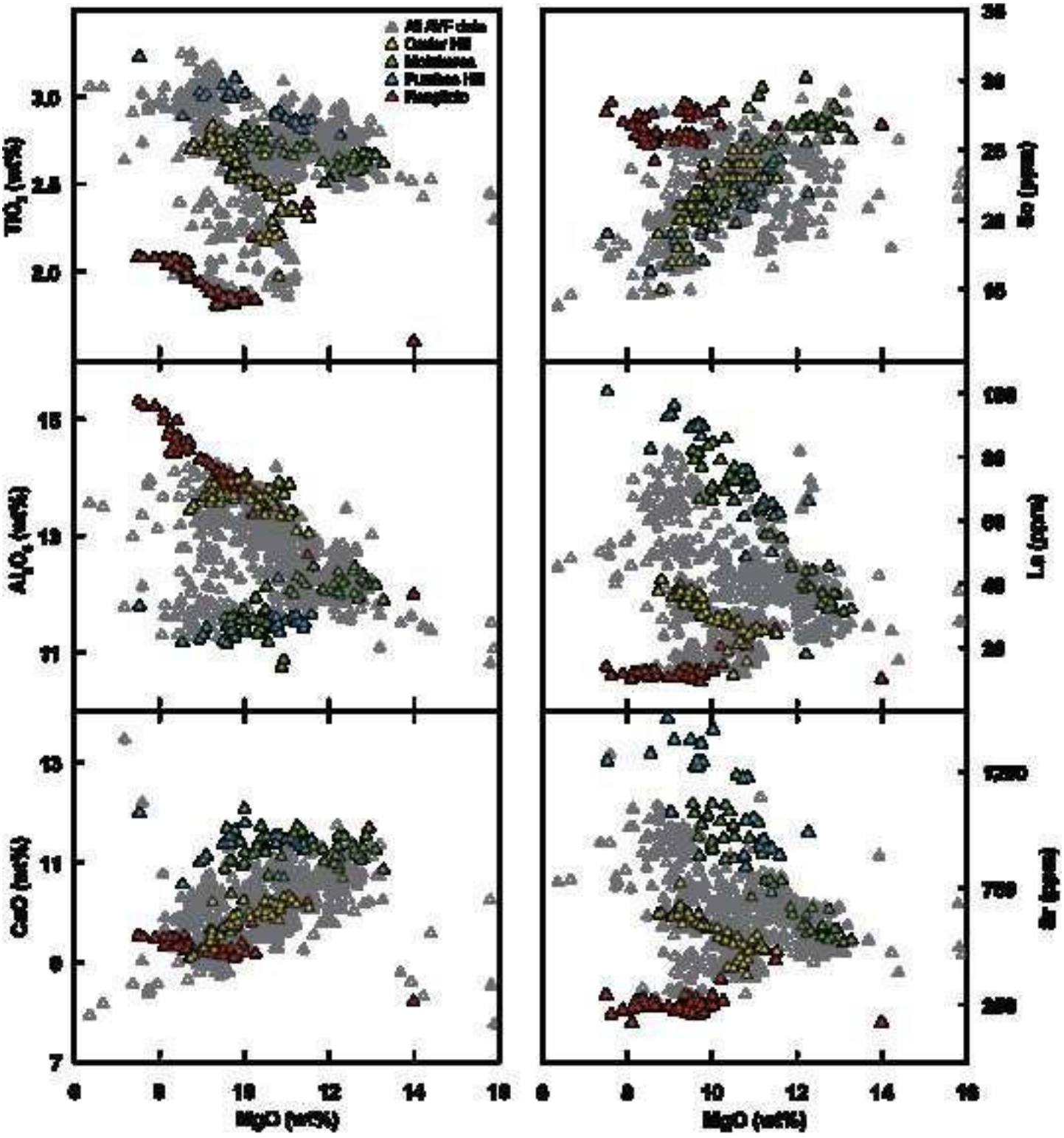

Figure 4

Click here to download Figure Figure 4.png

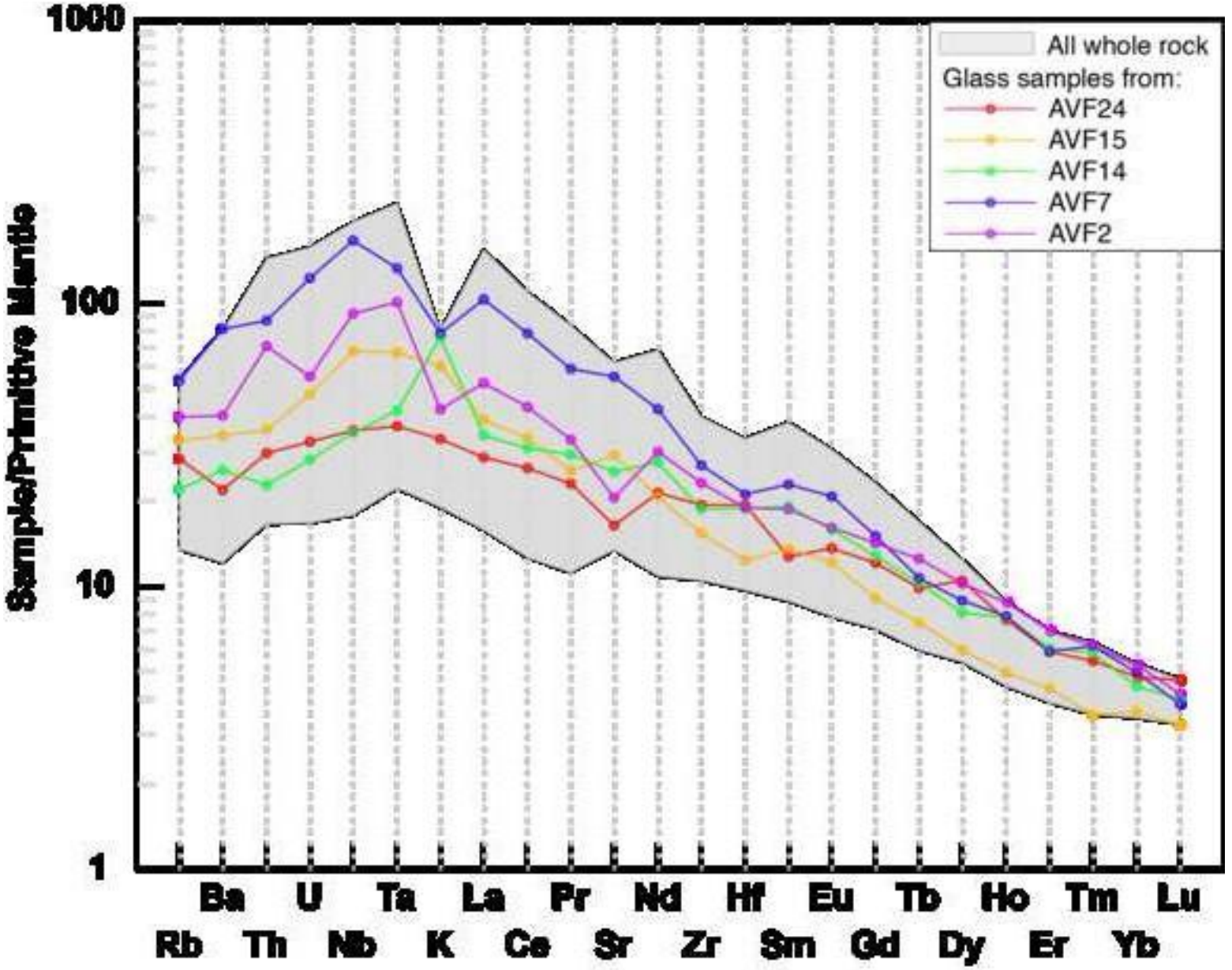

Figure 5

Click here to download Figure Figure 5.png

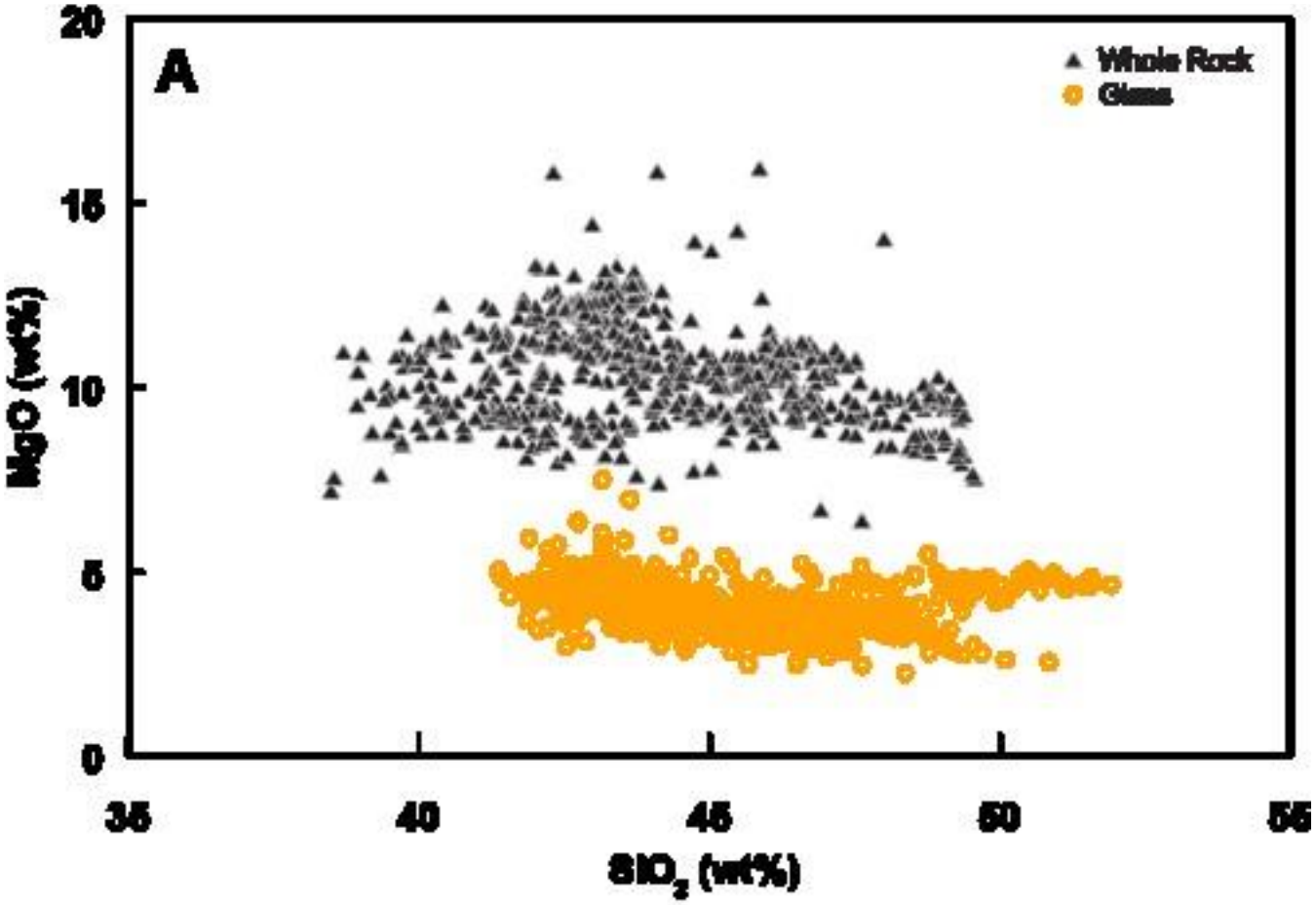

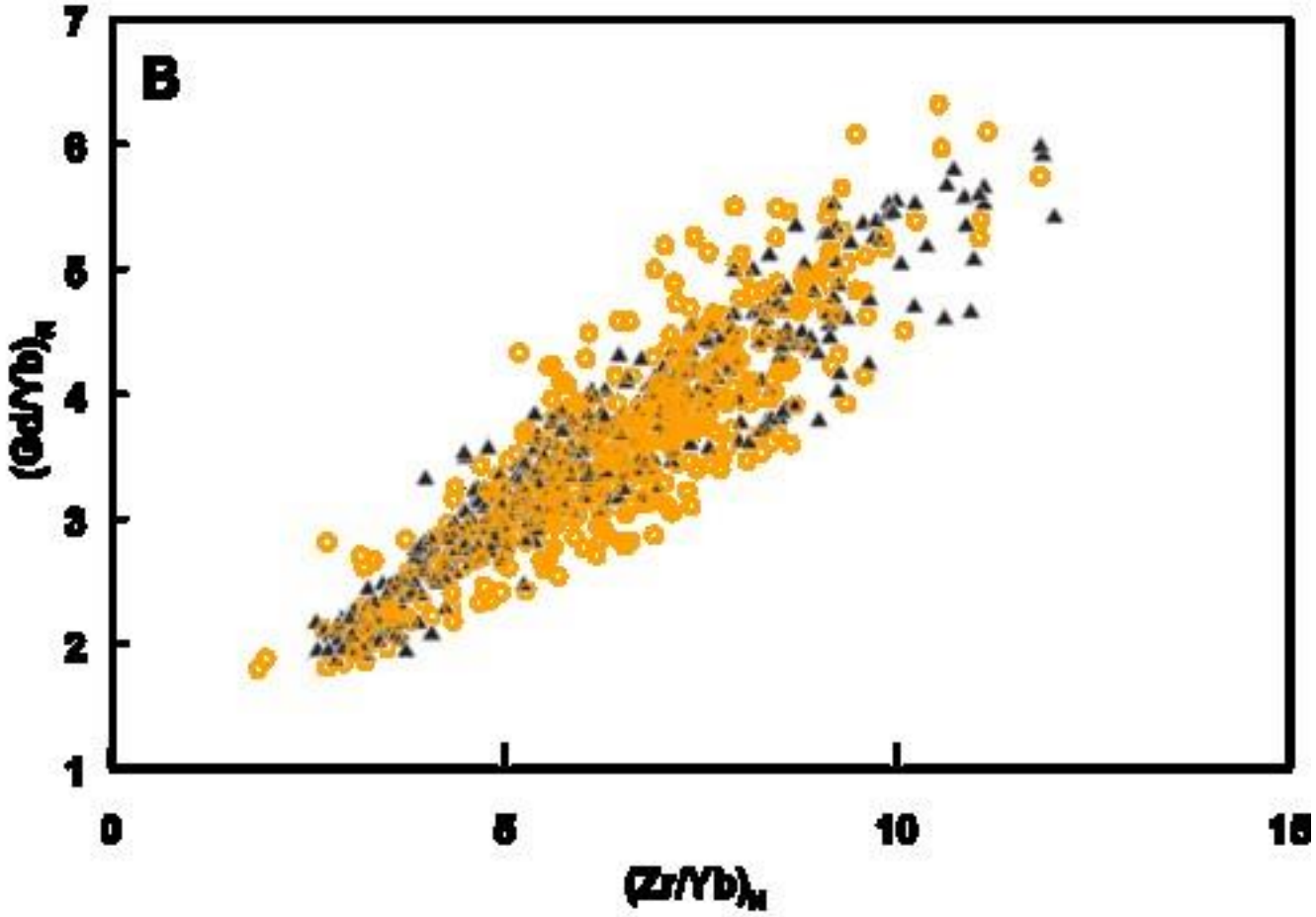

Figure 6

Click here to download Figure Figure 6.png

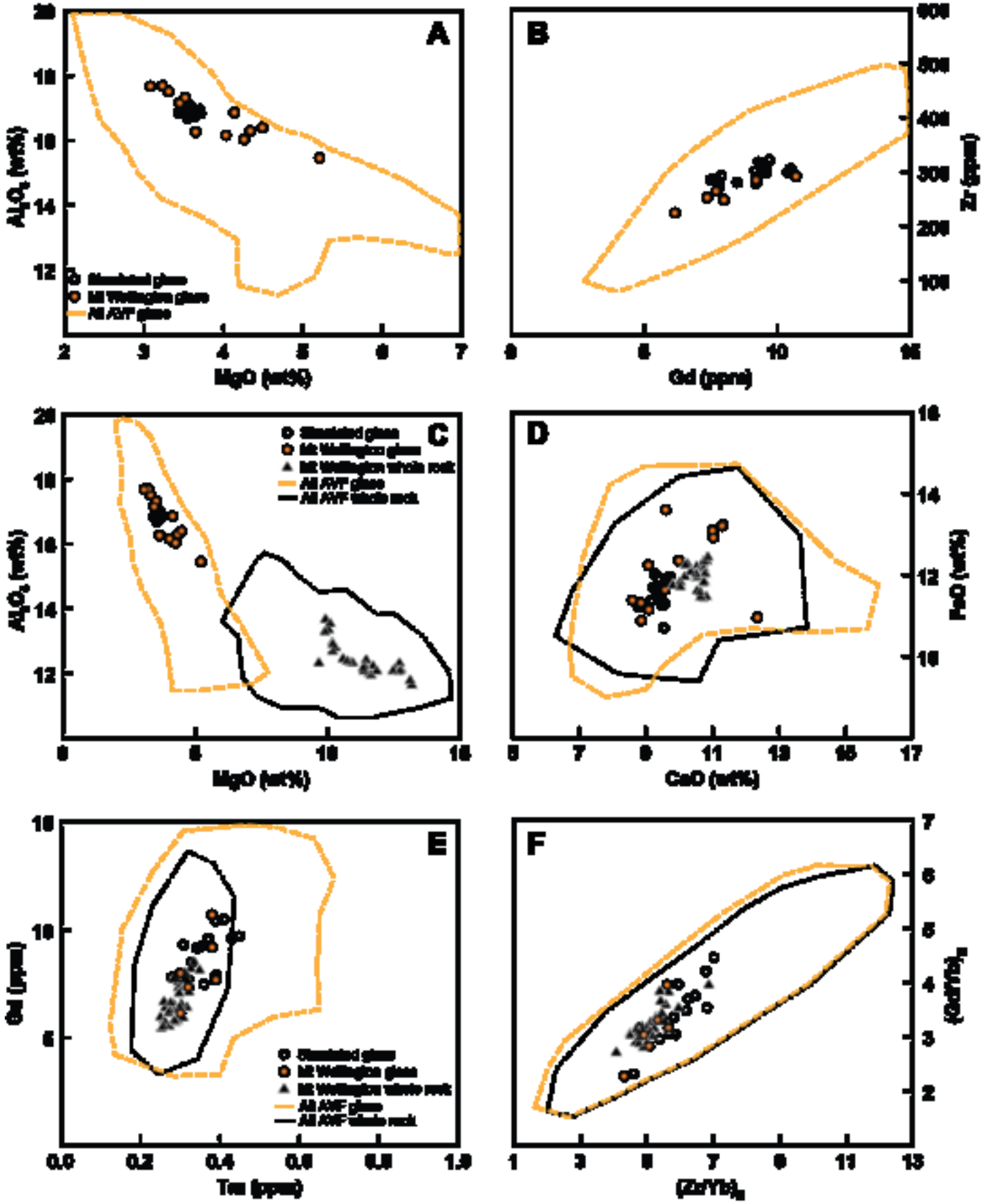

Figure 7

Click here to download Figure Figure 7.png

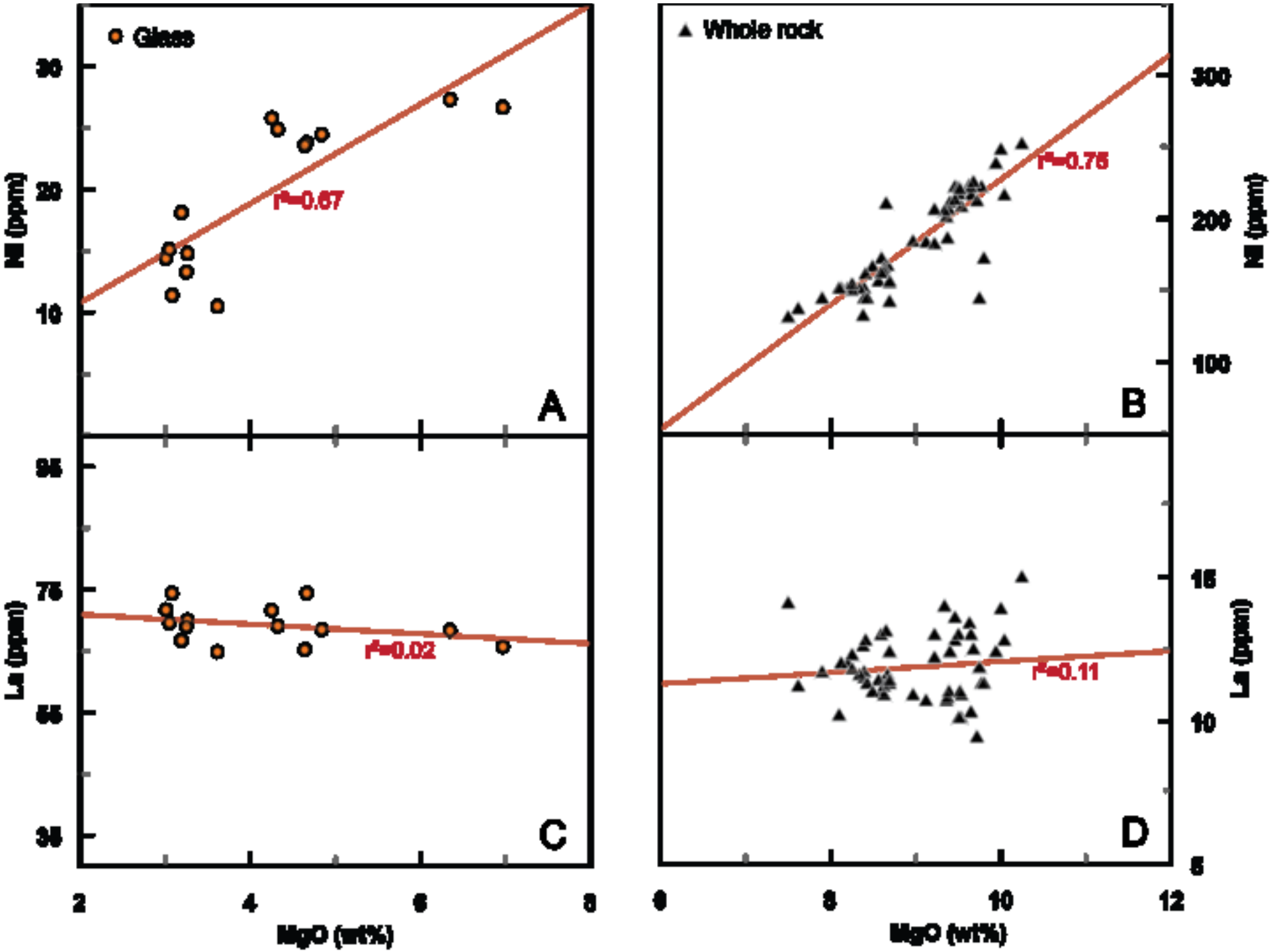

Figure 8

Click here to download Figure Figure 8.png

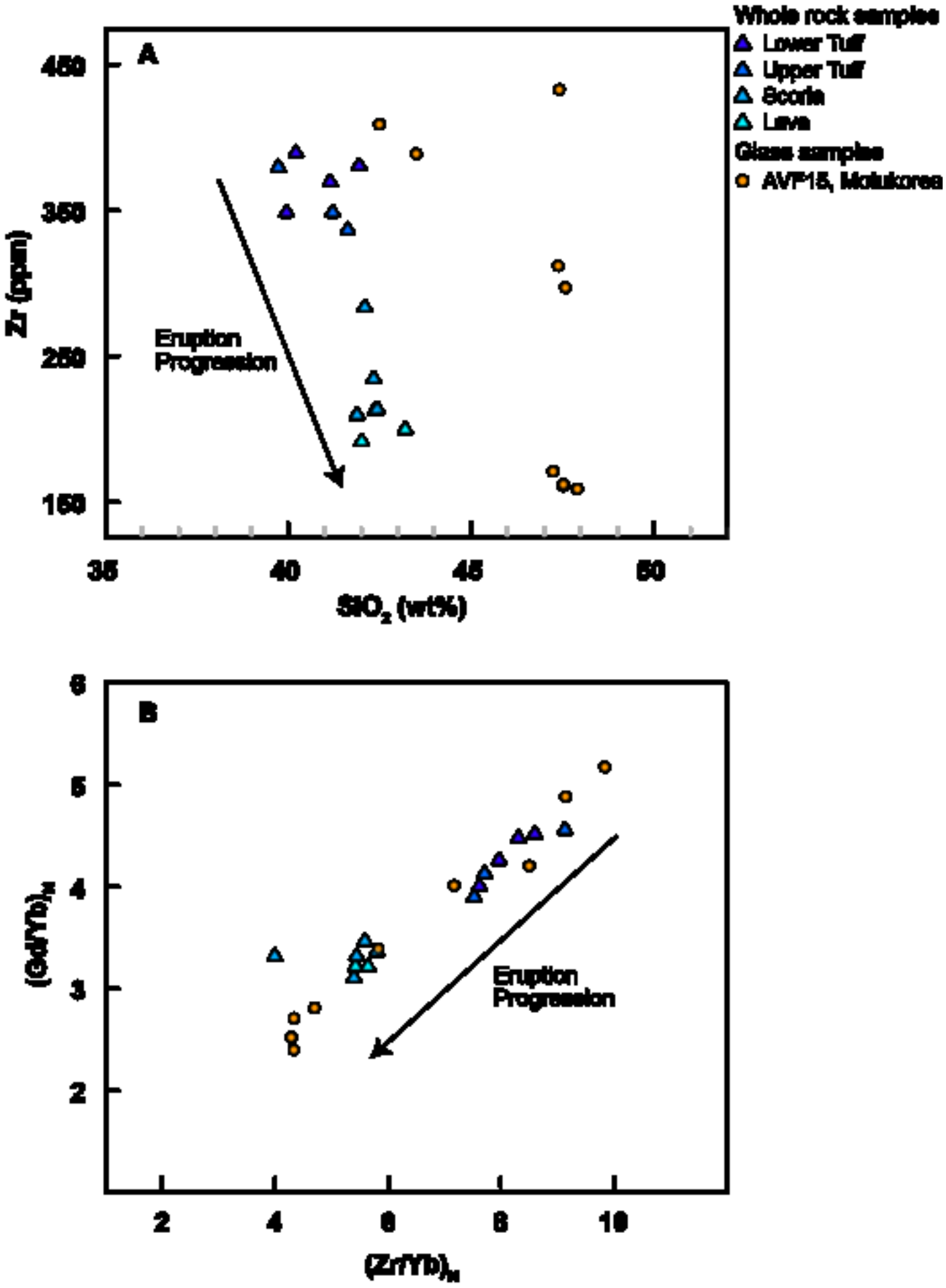

Figure 9

Click here to download Figure Figure 9.png

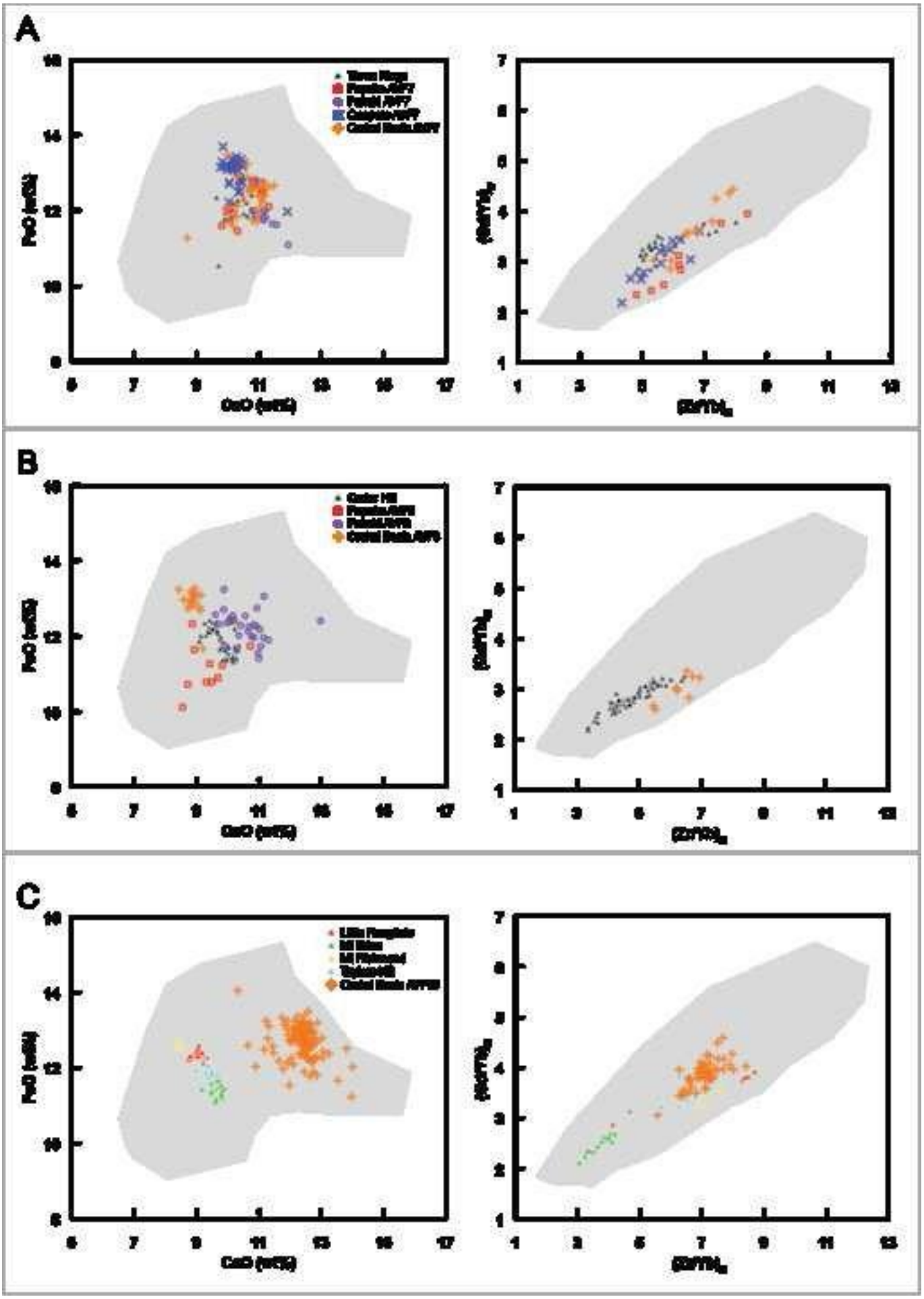

Figure 10

Click here to download Figure Figure 10.png

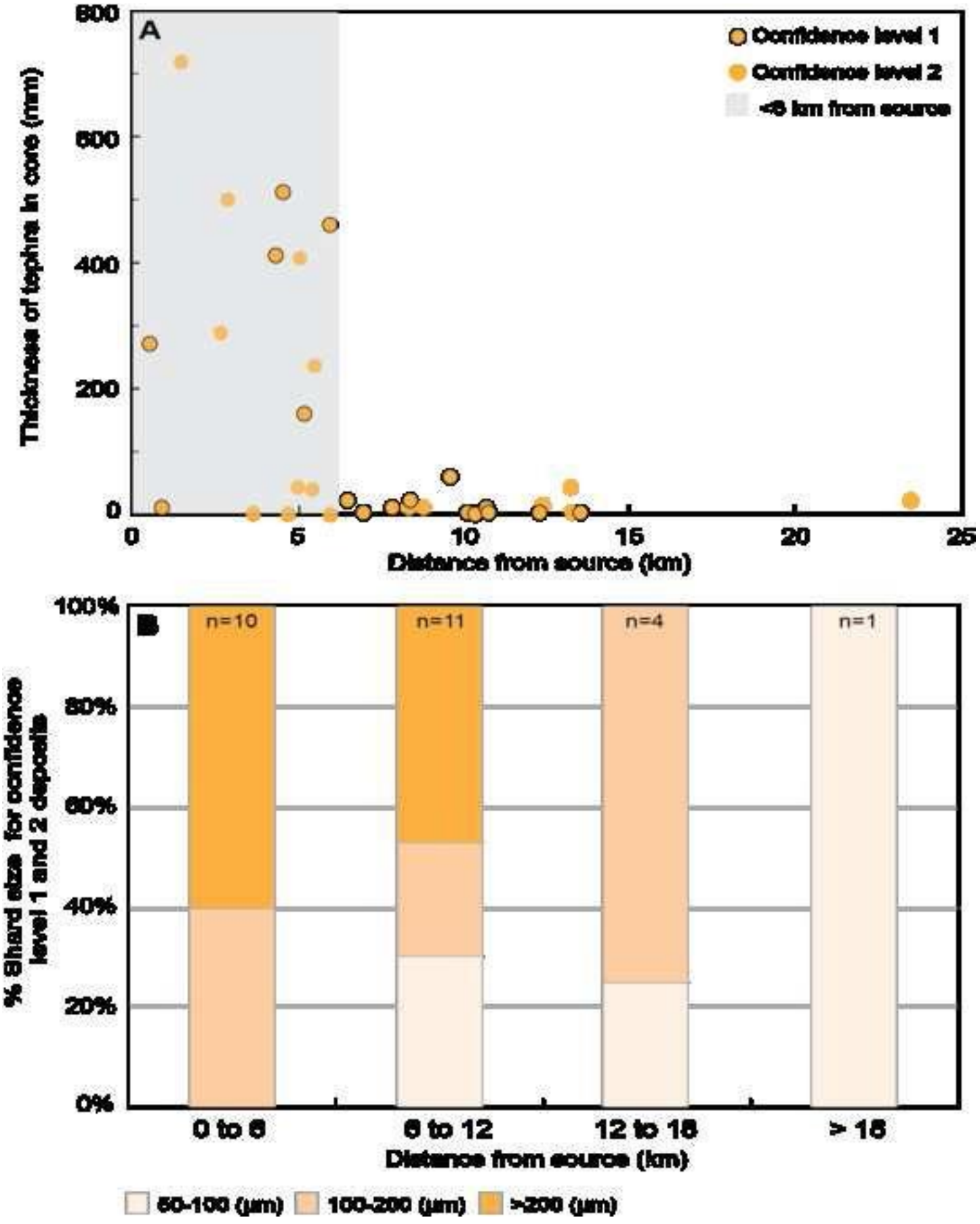

Figure 11

Click here to download Figure Figure 11.png

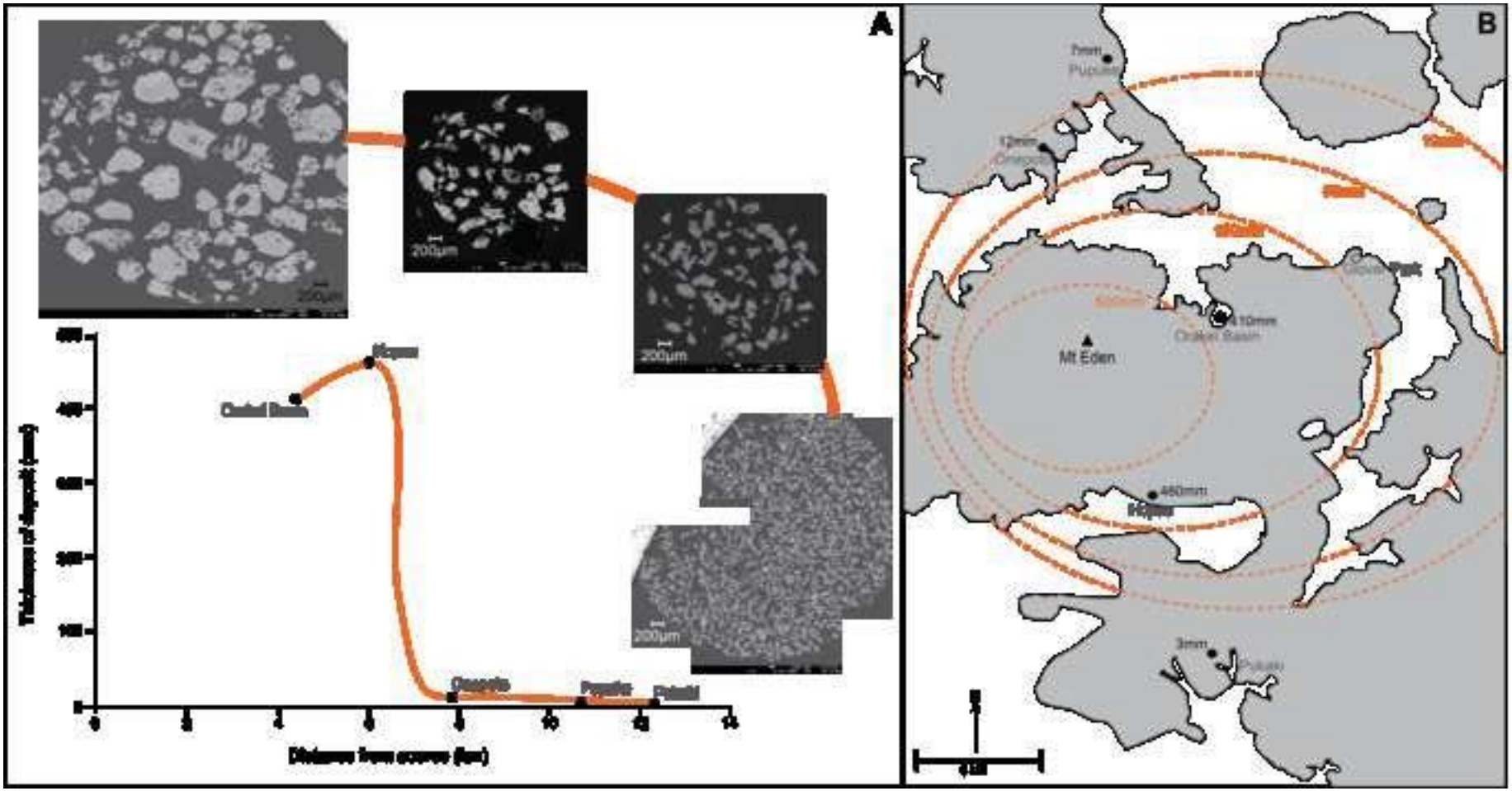

Figure 12

Click here to download Figure Figure 12.png

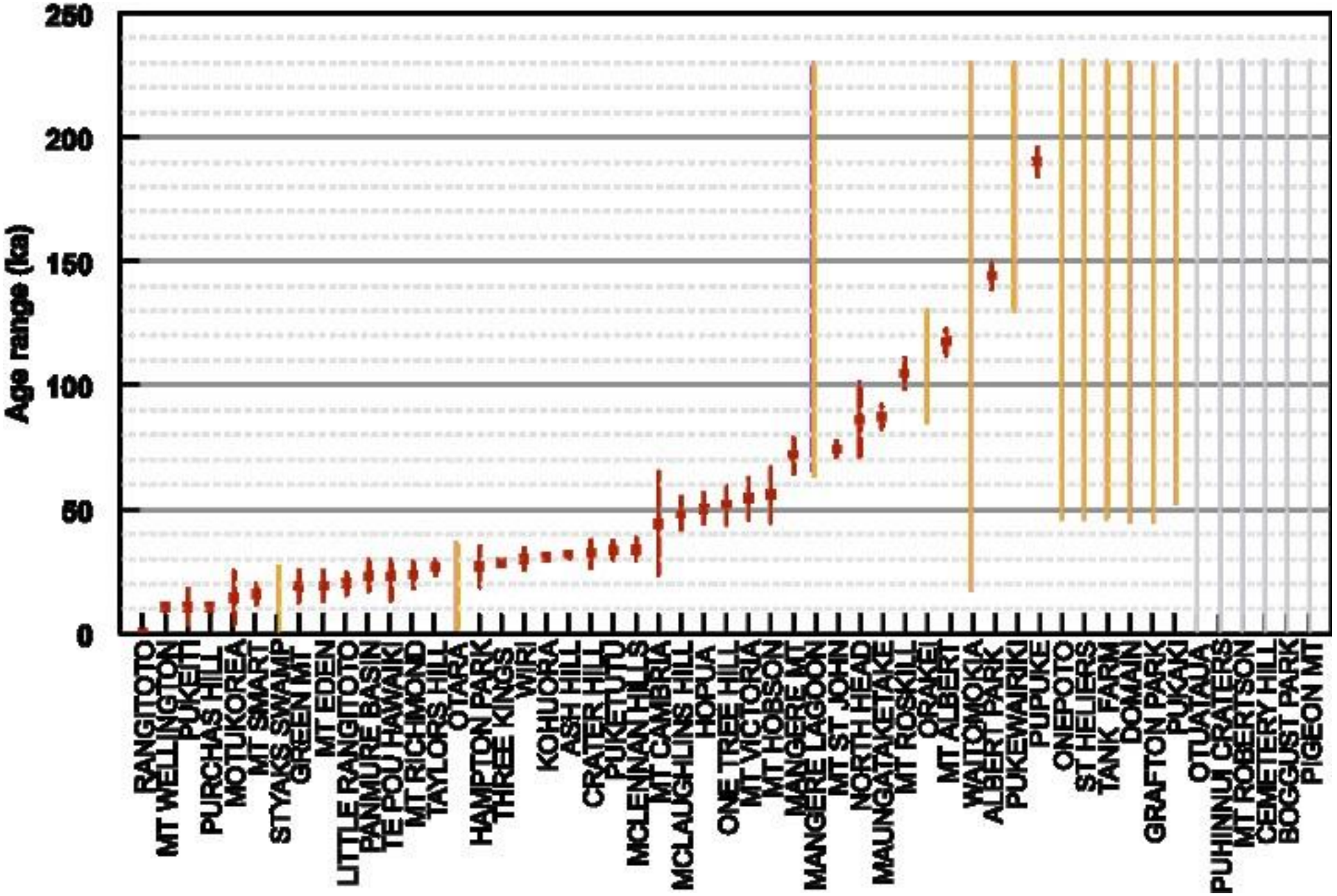

Figure 13

Click here to download Figure Figure 13.png

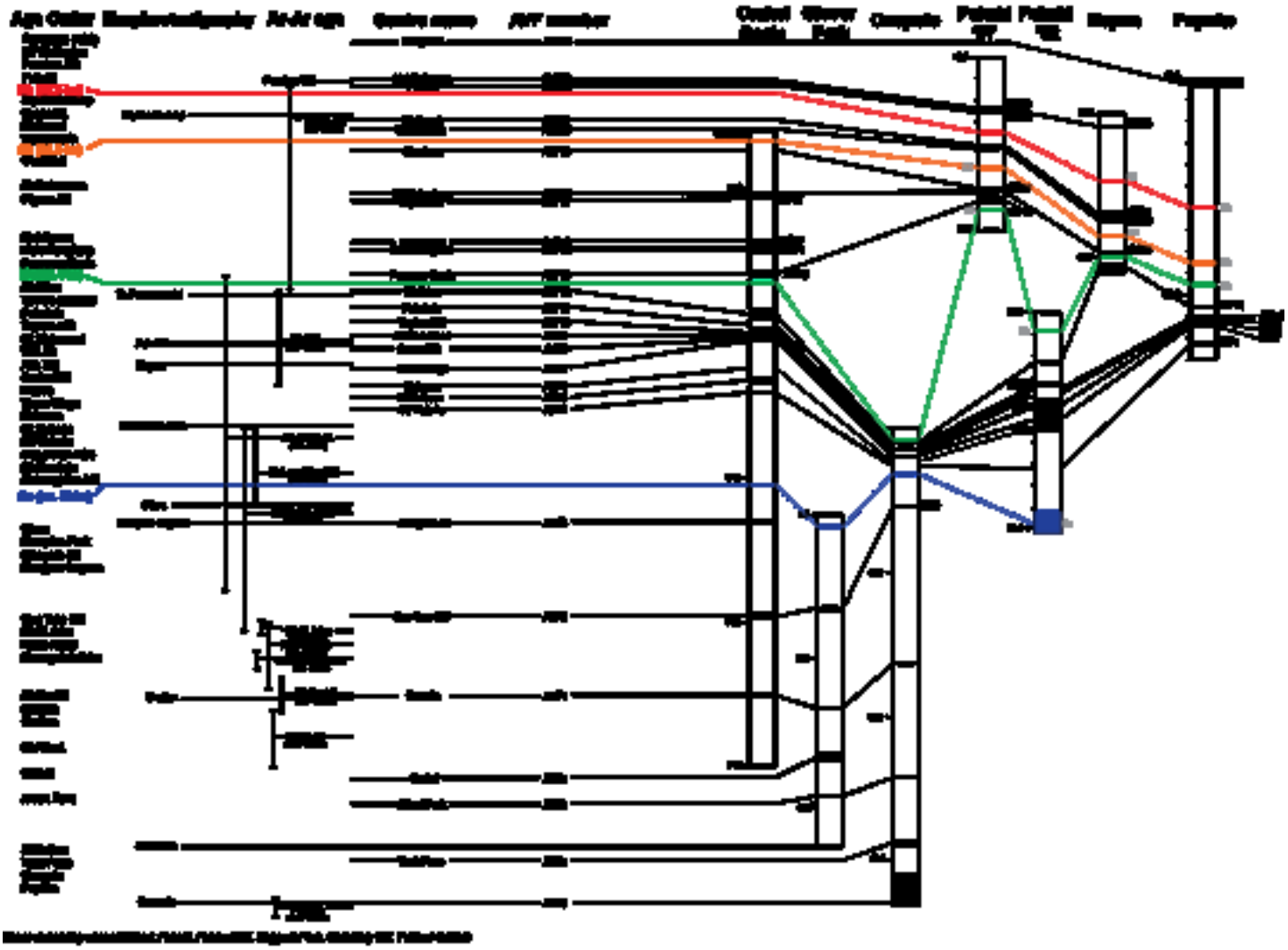

Figure 14

Click here to download Figure Figure 14.png

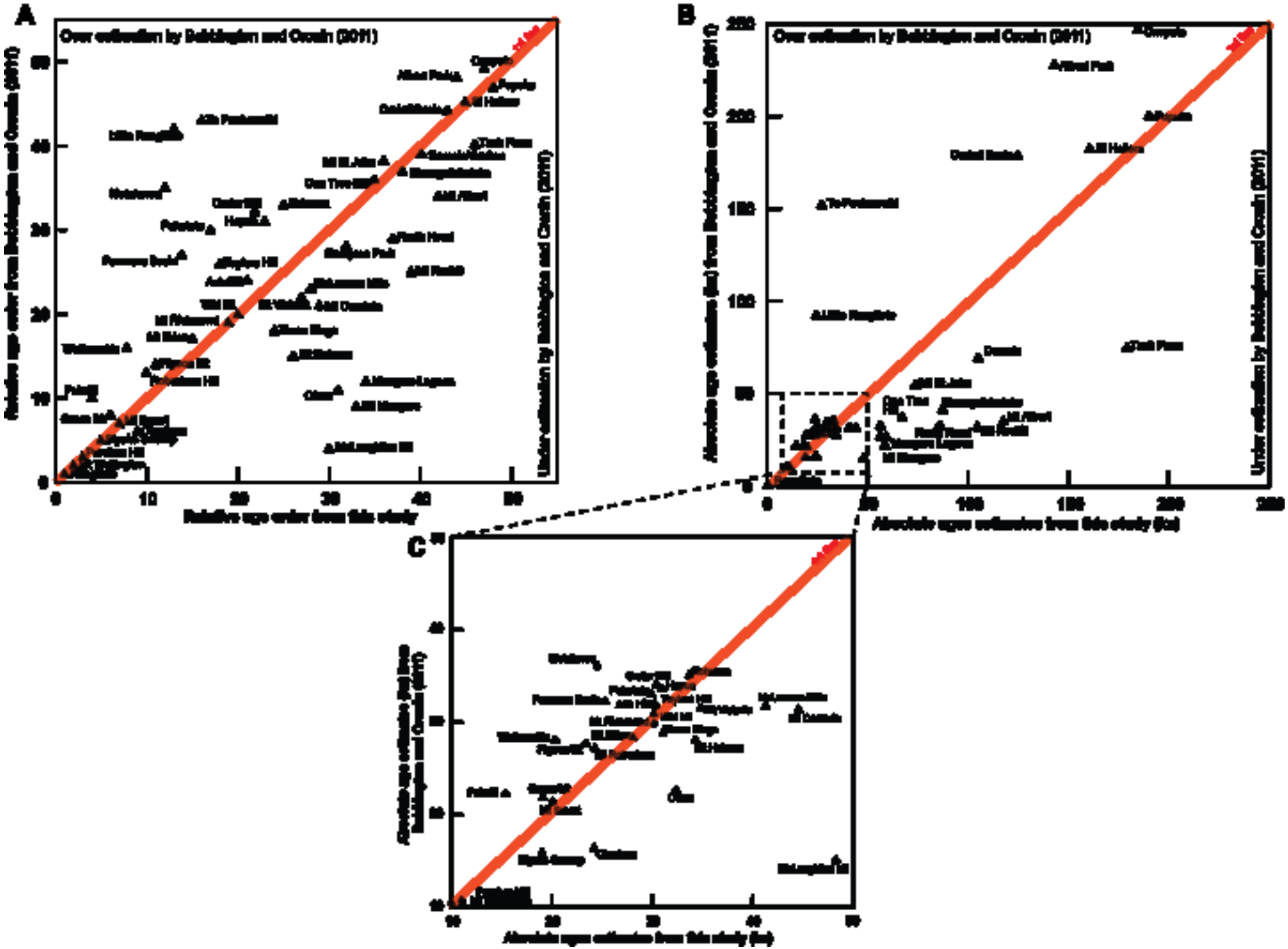

Figure 15

Click here to download Figure Figure 15.png

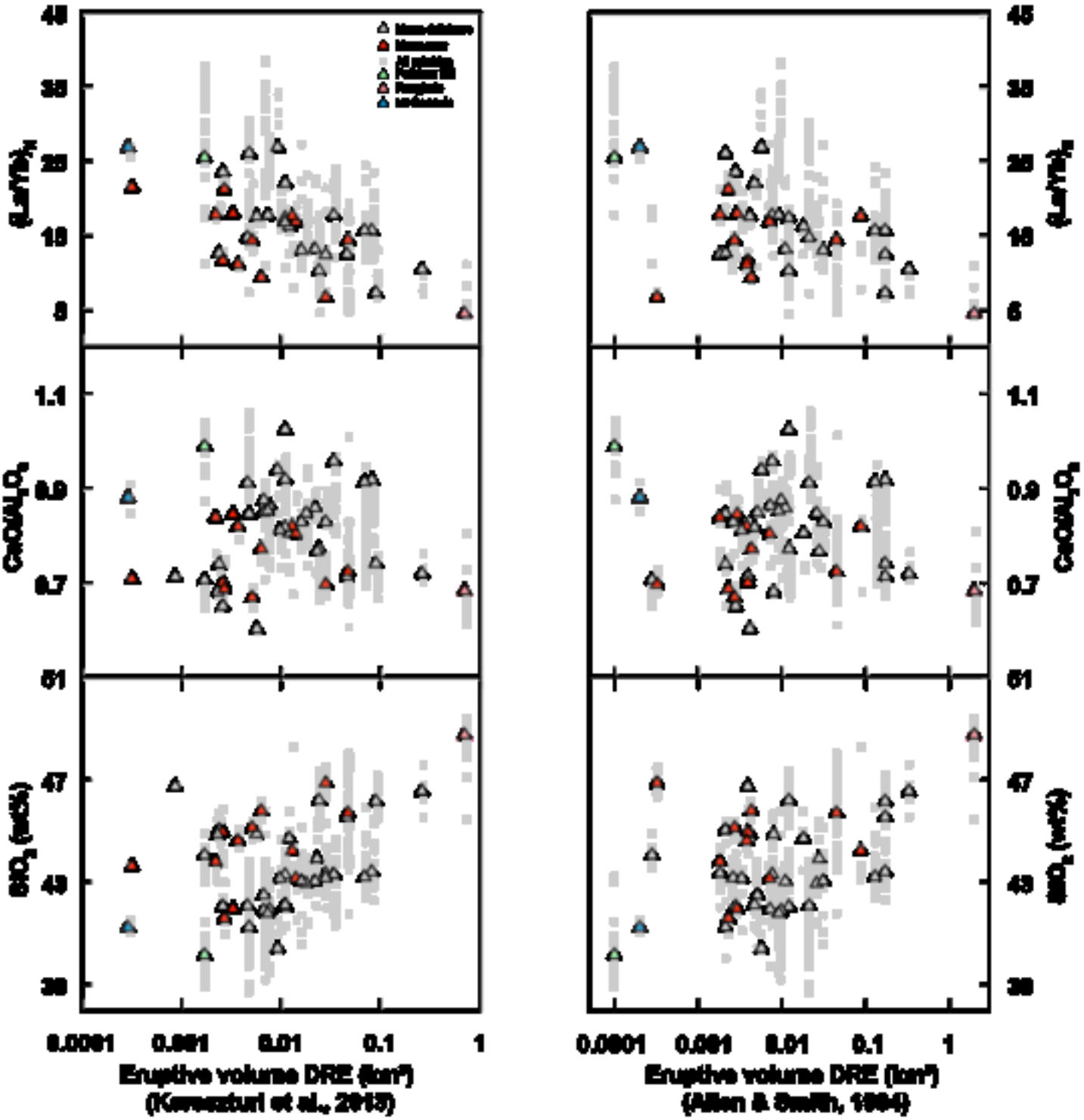

Table 1

Centre	Current whole rock data		References
	Major	Trace	
ALBERT PARK	4	4	McGee, 2012; Smith unpub data
ASH HILL	0	0	
BOGGUST PARK	0	0	
CEMETERY HILL	0	0	
CRATER HILL	61	61	Smith et al. 2008
DOMAIN	19	7	Smith unpub data
GRAFTON PARK	10	10	DEVORA group unpub data
GREEN HILL	3	1	Miller, 1996
HAMPTON PARK	4	0	Miller, 1996
HOPUA	1	1	Smith unpub data
KOHUORA	0	0	
LITTLE RANGITOTO	17	1	Franklin, 1999; Smith unpub data
MANGERE LAGOON	0	0	
MANGERE MT	7	2	Miller, 1996
MAUNGATAKETAKE	23	23	Smith unpub data
MCLAUGHLINS HILL	1	0	Heming and Barnet, 1986
MCLENNAN HILLS	6	3	Miller, 1996
MOTUKOREA	53	53	Bryner, 1991; McGee, 2012, McGee et al. 2012
MT ALBERT	2	4	Smith unpub data
MT CAMBRIA	1	1	Smith unpub data
MT EDEN	29	17	Eade, 2009; McGee, 2012
MT HOBSON	10	2	Smith unpub data
MT RICHMOND	6	3	Eade, 2009; McGee, 2012; Smith unpub data
MT ROSKILL	3	2	McGee, 2012
MT SMART	2	2	McGee, 2012; Smith unpub data
MT ST JOHN	22	13	Franklin, 1999; Eade, 2009
MT VICTORIA	4	2	Smith unpub data
MT WELLINGTON	34	34	McGee, 2012, McGee et al. 2013
NORTH HEAD	6	5	Smith unpub data
ONE TREE HILL	8	4	Eade, 2009; Smith unpub data
ONEPOTO	0	0	
ORAKEI	41	21	Franklin, 1999; Smith unpub data
OTARA	12	0	Miller, 1996; McGee, 2012
OTUATAUA	1	1	Heming unpub data
PANMURE BASIN	22	21	Smith unpub data
PIGEON MT	1	1	Smith unpub data
PUHINUI CRATERS	0	0	
PUKAKI	2	2	Zawalna-Geer, 2012
PUKEITI	1	1	Smith unpub data
PUKEKIWIRIKI	4	3	Smith unpub data
PUKETUTU	23	13	Miller, 1996; McGee, 2012
PUPUKE	51	51	Spargo, 2007

PURCHAS HILL	27	27	McGee 2012; McGee et al. 2013
RANGITOTO	55	55	Hookway, 2000; Needham et al. 2011
ROBERTSON HILL	0	0	
ST HELIERS	1	1	Smith unpub data
STYAKS SWAMP	0	0	
TANK FARM	0	0	
TAYLOR'S HILL	3	3	McGee, 2012; Smith unpub data
TE POU HAWAIKI	13	0	Franklin, 1999
THREE KINGS	36	35	Eade, 2009; Smith unpub data
WAITOMOKIA	9	9	McGee, 2012
WIRI	12	12	McGee, 2012; McGee et al. 2013
TOTALS	**650**	**511**	

This study whole rock data	
Major	Trace
Surface exposure currently	non-existent
3	3
new centre	
	2
	4
Surface exposure currently	non-existent
Surface exposure currently	non-existent
6	6
	3
5	5
	3
1	1
5	5
5	5
6	6
6	6
	1
	2
2	2
	5
5	5
5	5
new centre	
4	4
4	4
	2
1	1

2	2
4	4
2	2
Surface exposure currently non-existent	
Surface exposure currently non-existent	
6	6
5	5
77	**99**

Table 2

Table*. Over view of current volcanoes identified in the Auckland Volcanic Field, their age, relative age and Dense Rock Equivalent (DRE) values and geochemical analyses.

Centre name	Eruption types[a]	Age estimate (ka) min 2sd	mean	max 2sd	Method	Method reference	Relative ages and relationships based on morphology	DRE volumes x10^6 m^3 Total	Tuff	Scoria Cone	Tephra
ALBERT PARK	A,B,C	141.3	146.9	152.5	Ar-Ar	Leonard et al. 2017		27.8	0.82	0.01	0.43
ASH HILL	A	31.4	31.8	32.2	14C	Hayward, 2008	older than Wiri Mt[b]	0.076	0.05	0.00	0.03
BOGGUST PARK	A? (new)							0.32	0.18	0.00	0.09
CEMETERY HILL	(new)							0.24	0.14	0.00	0.07
CRATER HILL	A,B,C	26.7	32.1	37.5	Ar-Ar	Cassata et al. 2008	Mono Lake' p.mag excursion[j], younger than Kohuora[a]	24.5	5.88	0.76	4.09
DOMAIN	A,B	52.0			Rotoehu Tephra in drill core		younger than Grafton Park[a,] one of the older centres in the AVF[g]	11.4	4.06	0.06	2.11
GRAFTON PARK	A,B	52.0			morphostratigraphy		older than Domain[a,] one of the older centres in the AVF[g]	11.4	4.06	0.06	2.11
GREEN MT	A,B,C	13.0	19.6	26.2	Ar-Ar	Leonard et al. 2017	older than Styaks Swamp[a]	12.2	0.36	1.50	2.43
HAMPTON PARK	A,B,C	37.0	55.0	73.0	Ar-Ar	Cassata et al. 2008	unusual p.mag orientation[j], just older than Otara[a]	2.41	0.11	0.40	0.65
HOPUA	A	45.2	51.6	58.0	Ar-Ar	Leonard et al. 2017	younger than One Tree Hill[a]	0.86	0.31	0.00	0.15
KOHUORA	A	32.0	33.0	34.0	14C	Lindsay et al. 2011	older than Crater Hill[a], contains Kawakawa/Oruanui tephra (>25.4 ka)[h]	7.24	5.10	0.00	2.55
LITTLE RANGITOTO	B,C	16.3	20.7	25.1	Ar-Ar	Leonard et al. 2017	younger than Orakei[a]	1.71	0.00	0.50	0.75
MANGERE LAGOON	A,B	63.1			morphostratigraphy		just older than Mangere Mt[k]	2.04	0.71	0.01	0.37
MANGERE MT	B,C	63.1	70.3	77.5	Ar-Ar	Leonard et al. 2017	just younger than Mangere Lagoon[k], younger than One Tree Hill[a]	46.2	0.00	15.01	22.51
MAUNGATAKETAKE	A,B,C	84.1	88.9	93.7	Ar-Ar	Leonard et al. 2017	sea cut platform from last interglacial[a]	33.6	4.40	0.87	3.51
MCLAUGHLINS HILL	A,B,C	41.8	48.2	54.6	Ar-Ar	Leonard et al. 2017	older than Wiri Mt[a,b]	7.58	0.51	0.43	0.90
MCLENNAN HILLS	A,B,C	29.9	34.7	39.5	Ar-Ar	Leonard et al. 2017	Laschamp p.mag excursion[j], older than Mt Richmond[a]	21.9	0.42	3.79	5.90
MOTUKOREA	A,B,C	2.3	14.3	26.3	Ar-Ar	Leonard et al. 2017		4.56	0.66	1.31	2.30
MT ALBERT	A,B,C	113.6	119.2	124.8	Ar-Ar	Leonard et al. 2017	older than Mt Eden and Mt Roskill[a]	22.9	0.35	3.03	4.72
MT CAMBRIA	B,C	20.1	42.3	64.5	Ar-Ar	Leonard et al. 2017		0.29	0.00	0.29	0.44
MT EDEN	B,C	14.6	21.2	27.8	Ar-Ar	Leonard et al. 2017	much younger than Mt St John, younger than Three Kings, Mt Hobson[a], One Tree Hill and Domain[g]	89.8	0.00	5.94	8.92
MT HOBSON	B,C	45.3	56.9	68.5	Ar-Ar	Leonard et al. 2017	older than Three Kings[a]	6.68	0.00	1.20	1.80
MT RICHMOND	A,B	24.7	34.3	43.9	Ar-Ar	Leonard et al. 2017	Mono Lake' p.mag excursion[j], younger than McLennan Hills[a], older than Okaia tephra (28.6 ka)[d]	5.67	1.17	3.04	5.14
MT ROBERTSON	A,B							2.72	1.01	0.24	0.87
MT ROSKILL	A,B,C	99.1	105.3	111.5	Ar-Ar	Leonard et al. 2017	post-Blake p.mag excursion[j], younger than Mt Albert[a]	14.4	0.02	1.37	2.07
MT SMART	A,B,C	12.8	16.4	20.0	Ar-Ar	Leonard et al. 2017	younger than One Tree Hill[a]	13.4	0.00	2.34	3.52
MT ST JOHN	B,C	71.9	75.3	78.7	Ar-Ar	Leonard et al. 2017	much older than Mt Eden and Three Kings[a]	28.1	0.00	0.40	0.60
MT VICTORIA	B,C	42.8	57.6	72.4	Ar-Ar	Leonard et al. 2017		4.81	0.00	2.58	3.87
MT WELLINGTON	B,C	9.3	10.3	11.3	14C	Lindsay et al. 2011	just younger than Purchas Hill[a]	82.3	1.93	3.02	5.49
NORTH HEAD	A,B	72.3	87.5	102.7	Ar-Ar	Leonard et al. 2017	raised sea levels ca. 128-116 ka[l]	2.65	1.12	0.04	0.61
ONE TREE HILL	B,C	45.2	52.8	60.4	Ar-Ar	Leonard et al. 2017	older than Hopua, Mt Hobson, Mt Eden, Mt Smart, Three Kings, One Tree Hill[a]	260	0.00	5.70	8.56
ONEPOTO	A	52.0			Rotoehu Tephra in drill core		similar age to Pupuke and Tank Farm[a]	2.62	1.54	0.00	0.77
ORAKEI	A	85.0		130.0	sed. rate ages of tephra horizons	Molloy et al. 2009	not breached in last interglacial, older than Little Rangitoto[a]	6.70	3.77	0.00	1.89
OTARA	A,B,C	0.0		73.0	morphostratigraphy		unusual p.mag orientation, just younger than Hampton Park[a]	2.30	0.11	0.70	1.10
OTUATAUA	A,B,C							6.30	0.00	0.99	1.49
PANMURE BASIN	A,B	17.5			Rerewhakaaitu tephra in drill core		older than Rerewhakaaitu (17 ka[e])	7.44	4.65	0.30	2.77
PIGEON MT	A,B,C							3.31	1.33	0.28	1.08
PUHINUI CRATERS	A? (new)							-	-	-	-
PUKAKI	A	52.0			Core extent			9.19	7.10	0.00	3.55
PUKEITI	B,C	4.2	11.4	18.6	Ar-Ar	Leonard et al. 2017	younger than Otuataua[a]	3.70	0.00	0.44	0.66
PUKETUTU	B,C	29.8	33.6	37.4	Ar-Ar	Cassata et al. 2008	paleomag excursion (32.4±0.3ka)	11.0	3.00	2.15	4.72
PUKEWAIRIKI	A,C	130.0			morphostratigraphy		sea cut platform from last interglacial[a]	17.5	2.29	0.00	1.15
PUPUKE	C,B,A	187.6	193.2	198.8	Ar-Ar	Leonard et al. 2017	similar age to Tank Farm and Onepoto[a]	46.7	20.11	0.00	10.06
PURCHAS HILL	A,B	10.7	10.9	11.1	14C	Lindsay et al. 2011	just older than Mt Wellington[a]	1.68	0.21	0.03	0.14
RANGITOTO 2	A,B,C	0.494	0.504	0.514	14C	Needham et al. 2011	youngest in the field[a]	699	4.65	41.60	64.73
RANGITOTO 1	A,B,C	0.539	0.553	0.567	14C; Needham et al. 2	Needham et al. 2011					
ST HELIERS	A,	52.0			Rotoehu Tephra in drill core			2.20	1.23	0.00	0.62
STYAKS SWAMP	A,	0.0		24.5	morphostratigraphy		just younger than Green Mt[a]	0.37	0.25	0.00	0.12
TANK FARM	A	52.0			morphostratigraphy		similar age to Onepoto and Pupuke[a]	5.87	4.13	0.00	2.06
TAYLORS HILL	A,B,C	24.2	27.4	30.6	Ar-Ar	Leonard et al. 2017	Mono Lake' p.mag excursion[j]	5.07	0.47	0.18	0.51
TE POU HAWAIKI	B	14.6			morphostratigraphy		older than Mt Eden[c]	28.1	0.00	0.08	0.12
THREE KINGS	A,B,C	27.7	28.7	29.7	14C	Lindsay et al. 2011	younger than One Tree Hill, Mt St John, Mt Hobson, older than Mt Eden[a]	69.3	0.00	3.00	4.51
WAITOMOKIA	A,B	15.6			morphostratigraphy		core contains Rotorua tephra, older than Pukeiti[a]	9.79	2.30	0.11	1.31
WIRI	A,B,C	25.6	30.2	34.8	Ar-Ar	Cassata et al. 2008	Mono Lake' p.mag excursion[j], younger than Ash Hill[b]	16.4	0.08	0.86	1.34

Table 3

Source	abv	Age	error	ref	interpreted age (yr)	error	95% confidence limits	
AVF24 [P48]*	Ra2	504	5	a				
AVF24 [P49]*	Ra1	553	7	a				
Taupo	Tp	1,718	30	b				
Tuhua	Tu	6,577	547	b				
Mamaku	Ma	7,940	257	b				
Rotoma	Ro	9,423	120	b				
AVF23					9,950	300	9,650	10,240
Opepe	Op	9,991	160	b				
Waiohau	Wh	14,009	155	b				
AVF22					15,310	650	14,660	15,960
Rotorua	Rr	15,635	412	b				
Rerewhakaiaitu	Rk	17,496	462	b				
AVF21					20,080	100	19,080	21,070
AVF20					20,310	142	18,890	21,740
Okareka	Ok	21,858	290	b				
AVF19					24,200	880	23,320	25,090
AVF18					24,260	400	23,860	24,650
AVF17					23,350	350	23,000	23,700
AVF15					24,410	290	24,120	24,700
AVF14					24,550	290	24,270	24,840
Te Rere	Tr	25,171	964	b				
AVF16					25,230	860	24,370	26,090
AVF13					25,230	310	24,920	25,540
Kawakawa/Oruanui	Kk	25,358	162	b				
AVF12					28,030	260	27,760	28,290
Okaia	O	28,621	1428	b				
AVF11					29,770	2240	27,530	32,010
AVF10					30,200	120	30,080	30,320
AVF9					30,200	2080	28,120	32,280
AVF8					30,400	400	30,000	30,810
AVF7					31,040	900	30,140	31,940
AVF6					33,710	1160	32,550	34,870
AVF5					34,200	860	33,340	35,070
AVF4					34,780	2000	32,780	36,780
Maketu	Mk	36,320	575	c				
Tahuna	Ta	39,268	1193	c				
Rotoehu	Re	52,000	7000	d				
AVF3					*59,230*	*10,230*	*49,000*	*69,460*
AVF2					*67,200*	*6,250*	*60,950*	*73,450*
AVF1					*106,170*	*4,300*	*101,870*	*110,470*
AVFa					*126,150*	*3,320*	*122,830*	*129,470*
AVFb					*144,870*	*2,400*	*142,470*	*147,270*
AVFc					*181,430*	*580*	*180,850*	*182,010*
AVFd		193,200	2,800	e				

Table 4

Core	Sample name	New Horizon#	Depth (m)	Thickness (mm)	Average age (ka)	Proposed Centre(s)	Confidence level	Correlation criteria				Alternative(s)	Confidence level	Correlation criteria			
								Age	Chem	Scale	Location			Age	Chem	Scale	Location
Post Rerewhakaitu (<17.5ka)																	
Pupuke	T21-1-48/58929	24	57.90	22	0.6	**Rangitoto**	**1**	✓	✓	✓	✓	-	-				
Hopua	T4-2-H1-2/58839	23	38.95	3	9.95 ± 0.3	**Mt Wellington**	**1**	✓	✓	✓	✓						
Pukaki	T14 47.72m	22	47.72	1.0	15.31 ± 0.65	**Pukeiti**	**2**	✓		✓	✓	-	-				
Rerewhakaitu to Okareka (17.5 - 21.9ka)																	
Pukaki	AT209 49.15m	21	49.15	3.0	20.08 ± 0.1	**Mt Smart**	**2**	✓	✓	✓	✓	Mt Eden	3	✓			✓
Hopua	T5-2-H1-18/58855(-58856)	21	45.17	290								Panmure Basin	2		✓	✓	
												Boggust Park	3	?		✓	✓
Pukaki	AT210 49.17m	20	49.17	2.0	20.3 ± 0.14	**Waitomokia**	**2**	✓	✓	✓	✓	Mt Robertson	3	?		✓	✓
Hopua	T6-5-H1-20/58857(-58858)	20	45.51	235								Otuataua	3	?		✓	✓
Okareka to Oruanui (21.9- 25.4ka)																	
Pukaki	T43 51.05	19	51.05	1.0	24.2 ± 0.88	**Otuataua**	**3**	?		✓	✓	Wiri Mt	3	✓		✓	
												Boggust Park	3	?		✓	✓
												Mt Robertson	3	?		✓	✓
Orakei Basin	OB1.#50-4-44.22	18	44.22	8		**Mt Robertson**	**3**	?		✓	✓	Panmure Basin	3	✓			✓
Hopua	T5-6-H1-32-58869	18	47.81	40	24.26 ± 0.4							Boggust Park	3	?			✓
Pukaki	T45 51.19	18	51.19	0.5													
Orakei Basin	OB1.#50-6-44.652(-44.654)	17	44.65	5	23.35 ± 0.35	**Pigeon Mt**	**3**	?	✓	✓	✓	Little Rangitoto	3	✓	✓		
												Motukorea	2	✓	✓	✓	✓
												Mt Cambria	3	✓			✓
												Panmure Basin	3	✓			
												Taylors Hill	3	✓			✓
Orakei Basin	OB1.#50-6-47.715	15	47.72	12	24.41 ± 0.29	**Motukorea**	**2**	✓	✓	✓	✓	Pigeon Mt	3	?	✓	✓	✓
												Mt Cambria	3	✓			✓
Orakei Basin	OB1.#33-2-48.12(-48.128)	14	48.13	12	24.55 ± 0.29	**Little Rangitoto**	**1**	✓	✓	✓	✓	-	-				
Orakei Basin	OB1.#33-2-48.19(-48.276)	newB	48.28	10		**?**											
Orakei Basin	OB1.#33-4-49.14(-49.46)	newA	49.46	45		**?**											
Orakei Basin	OB1.#34-3-50.089(-49.554)	13	50.09	160	25.23 ± 0.86	**Panmure Basin**	**1**	✓	✓	✓	✓	Mt Eden	2	✓			✓
Pukaki	T42/45 51.52	13 (16)	51.52	50.0								Little Rangitoto	2	✓			✓
												Mt Richmond	2	✓			✓
												Taylors Hill	2	✓			
Oruanui to Rotoehu (25.4 - ca. 52 ka)																	
Orakei Basin	OB1.#36-2-52.817(-53.029)	12	53.03	410								Three Kings	2	✓		✓	✓
Onepoto	On2.#4-39.06	12	36.09	12								Te Pou Hawaiki	3		✓		✓
Pukaki	54.355m	12	54.36		28.03 ± 0.26	**Mt Eden**	**1**	✓	✓	✓	✓						
Pupuke	P23/58947	12	67.59	7													
Hopua	T6-3-H1-39/58876	12	48.80	460													
Pukaki	c. 55.355m	11	55.34	< 10	29.8 ± 2.2	**Puketutu**	**2**	✓	✓	✓	✓	Kohuroa	3	✓			✓
												Otuataua	3			✓	✓
												Mt Robertson	3			✓	✓
												Wiri Mt.	3	✓		✓	
Orakei Basin	OB1.#37-2-54.119(-54.313)	10	54.21	407								Panmure Basin	2	✓	✓	✓	
Onepoto	On2.#4-39.47	10	39.47	15	30.2 ± 0.12	**Taylor's Hill**	**2**	✓	✓		✓	Pigeon Mt	3	?	✓		✓
	T18-7-P26/58951	10	68.09	3								Three Kings	3	✓			
Pupuke												Mt Cambria	3	✓			
Pupuke	P27/58952	9	68.15	6	30.2 ± 2.08	**Mt Richmond**	**3**	✓		✓		Mt Cambria	3	✓			✓
												Mt Richmond	3	✓			✓
												Hopua	3		✓		✓
Orakei Basin	OB1.#37-2-54.97	8	54.27	45								Kohuora	2	✓			✓
Pupuke	P28/58953	8	68.24	20	30.4 ± 0.4	**Crater Hill**	**2**	✓	✓		✓						
Pukaki	c. 56.4m	8	56.40	ca. 720													
Orakei Basin	OB1.#37-2-54.304(AVF2)	7	54.34	20													
Onepoto	On2.#4-39.905(-39.914)	7	39.90	20	31.04 ± 0.9	**Three Kings**	**1**	✓	✓	✓	✓	-	-				
Pukaki	c. 56.8	7	56.90														
Pupuke	T19-3-P29/58954	7	68.49	2													
Pukaki	c. 57.0	6	57.10	ca. 500	33.71 ± 1.16	**Kohuroa**	**2**	✓		✓	✓	Crater Hill	2	✓	✓		✓
												Puketutu	2	✓	✓		✓
												Wiri Mt	3	✓			✓
												Mt Robertson	3	?		✓	✓
Orakei Basin	OB1.#39-3-57.349(-57.44)	5	57.34	110	34.2 ± 0.86	**Mt Hobson**	**3**		✓	✓	✓	Little Rangitoto	3			✓	✓
												Mt Cambria	3	✓			✓
												Mt St John	3			✓	✓
												Mt Victoria	3		✓	✓	✓
												North Head	3			✓	✓
												Panmure Basin	3			✓	✓
												Taylors Hill	3			✓	✓
Orakei Basin	OB1.#39-5-58.11(-58.07)	4	58.11	41	34.78 ± 2.0	**Mt Victoria**	**3**		✓	✓	✓	Little Rangitoto	3	✓		✓	✓
Pupuke	P33/58960	4	69.32	15								Mt Cambria	3	✓			✓
												Mt Hobson	3	✓			✓
												Mt St John	3				✓
												North Head	3			✓	✓
												Taylors Hill	3	✓			✓
Pre Rotoehu ca. 52 ka																	
Orakei Basin	OB1.#45-5-67.039(-61.17)	3	67.04	41	59 ± 10.0	**Mangere Mt**	**2**	✓	✓	✓	✓	Mt Cambria	3	✓			✓
												Mt Hobson	3	✓		✓	
												Mt Victoria	3	✓		✓	
												One Tree Hill	3	✓		✓	✓
Orakei Basin	OB1.#50-2-73.555	2	73.56	510													
Glover Park	GP6-8-10.38(-10.6)	2	10.60	60	67 ± 6.0	**One Tree Hill**	**1**	✓	✓	✓	✓	-	-				
Onepoto	On2.#6-2-43.66	2	43.66	4													
Orakei Basin	OB1.#54-3-80.047	1	80.05	100								Mt Roskill	3	✓			✓
Onepoto	AB1-On2-#11-51.30	1	54.30	15	106 ± 4.0	**Domain/Grafton**	**3**	?		✓	✓	North Head	3	✓			✓
Glover Park	GP16-17.52(&18.15)	1	18.15	12													
Glover Park	GP1/24 -20.78-21.0	AVFa	21.00	40	126 ± 3.0	**Orakei**	**2**	✓		✓	✓	Domain/Grafton	3	✓		✓	
												Mt Albert	3	✓		✓	
												Mt Roskill	3	✓		✓	
												North Head	3			✓	✓
Onepoto	On2.#18-62.36	AVFb	62.00	45	145 ± 2.0	**Albert Park**	**2**	✓	✓	✓	✓	Domain/Grafton	2	?	✓		✓
Glover Park	GP1/40 -23.67	AVFb	23.67	10													
Onepoto	On2.#21-66.68	AVFc	66.68	270	181 ± 0.6	**Tank Farm**	**1**	✓		✓	✓	Pupuke	3			✓	✓

Table 5

				Orakei Basin			Glover Park			Onepoto			Pukaki		Hopua			Pupuke		
Centre (eruption)	AVF#	Confidence level	DRE km^3 (2sf)	Distance to (km)	Horizon thickness (mm)	shard size (um)	Distance to (km)	Horizon thickness (mm)	shard size (um)	Distance to (km)	Horizon thickness (mm)	shard size (um)	Distance to (km)	Horizon thickness (mm)	Distance to (km)	Horizon thickness (mm)	shard size (um)	Distance to (km)	Horizon thickness (mm)	shard size (um)
Rangitoto	AVF24	1	0.70		n/a			n/a			n/a			n/a		n/a		8.4	22	>200
Mt Wellington	AVF23	1	0.082		n/a			n/a			n/a		10.4	1	7.0	3	>200		n/a	
Little Rangitoto	AVF14	1	0.0017	0.9	12	>200		n/a			n/a			n/a		n/a			n/a	
Panmure Basin	AVF13	1	0.0074	5.2	160	100-200		n/a			n/a			n/a		n/a			n/a	
Mt Eden	AVF12	1	0.090	4.4	410	>200		n/a		7.9	12	100-200	12.3	3	6.0	460	>200	10.7	7	50-100
Three Kings	AVF7	1	0.069	6.5	20	100-200		n/a		10.6	12	50-100	10.1	2		n/a		13.5	2	50-100
One Tree Hill	AVF2	1	0.26	4.6	510	>200	9.6	60	>200	10.8	4	100-200		n/a		n/a			n/a	
Tank Farm	AVFc	1	0.0059		n/a			n/a		0.6	270	>200		n/a		n/a			n/a	
Pukeiti	AVF22	2	0.0037		n/a			n/a			n/a		4.7	1		n/a			n/a	
Mt Smart	AVF21	2	0.013		n/a			n/a			n/a		7.0	3	2.7	290	>200		n/a	
Waitomokia	AVF20	2	0.010		n/a			n/a			n/a		3.7	2	5.5	235	100-200		n/a	
Motukorea	AVF15	2	0.0046	8.4	12	50-100		n/a			n/a			n/a		n/a			n/a	
Puketutu	AVF11	2	0.018		n/a			n/a			n/a		6.0	<10		n/a			n/a	
Taylors Hill	AVF10	2	0.0051	5.1	407	>200		n/a		12.4	15	100-200		n/a		n/a		13.2	3	100-200
Crater Hill	AVF8	2	0.024	13.2	45	100-200		n/a			n/a		1.5	720		n/a		23.5	20	<50
Kohuora	AVF6	2	0.0072		n/a			n/a			n/a		2.9	500		n/a			n/a	
Orakei Basin	AVFa	2	0.0067		n/a		5.4	40	100-200		n/a			n/a		n/a			n/a	
Albert Park	AVFb	2	0.028		n/a		8.8	10	50-100	5.0	45	100-200		n/a		n/a			n/a	

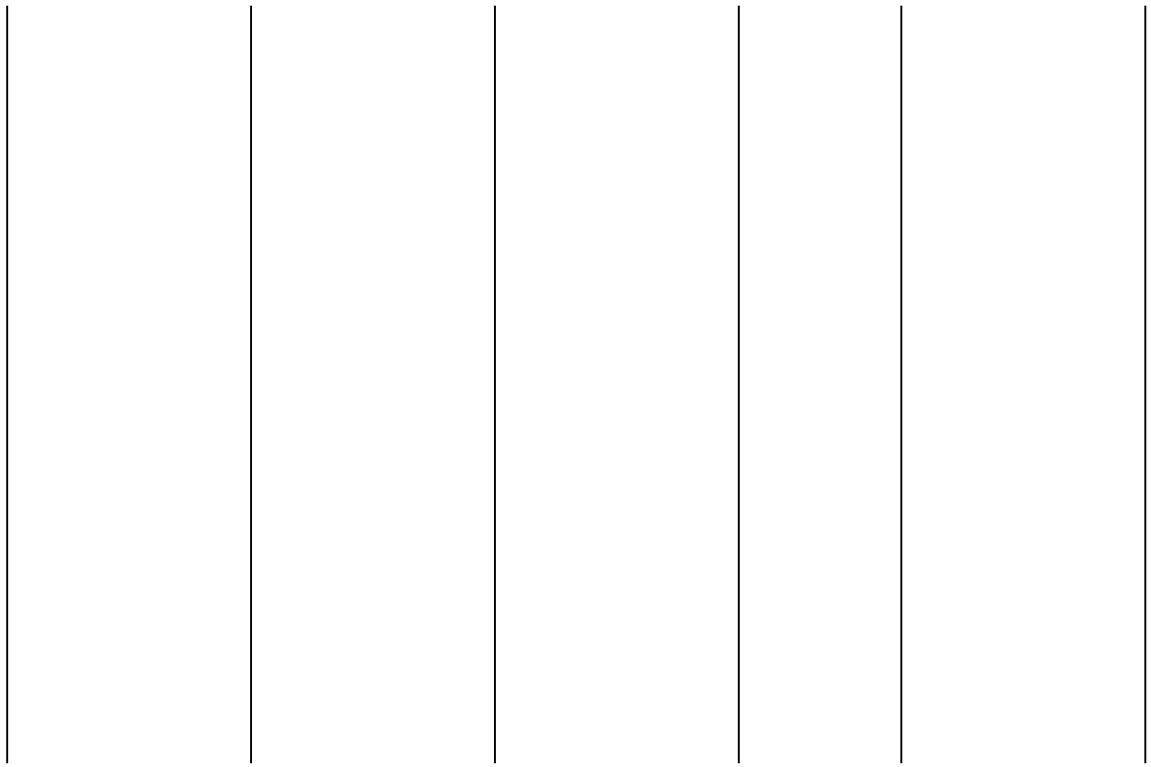

Table 6

Centre Name	Region	Total DRE volume (km^3)	Tephra thickness (cm)	Dispersal distance (km)
Paricutin	Michoacán-Guanajuanto volcanic field, Mexico	2.5	25	7
Sunset Crater	San Francisco volcanic field, Arizona	0.58	10	20
One Tree Hill	**Auckland volcanic field, New Zealand**	**0.26**	**6**	**9.6**
Mt Gambier	Newer Volcanics province, south-eastern Australia	0.198	≤5	10 to 12
Lanthrop Wells	Southwestern Nevada volcanic field	0.12	1	10
Cerro Negro*	Nicaragua	0.16	0.5	16
Three Kings	**Auckland volcanic field, New Zealand**	**0.069**	**2**	**6.5**
Marcath Volcano	Lunar Crater volcanic field, Central Nevada	0.06	2	7
Orakei Basin	**Auckland volcanic vield, New Zealand**	**0.0067**	**0.4**	**5.4**

Reference
Ort et al., 2008
Ort et al., 2008
This study
Lowe and Palmer, 2005; van Otterloo and Cas, 2013
Valentine et al., 2008
Hill et al., 1998
This study
Johnson et al., 2014
This study

Table 7

Relative Order	Centre Name	Mean age (t) in ka	Error (1sd)	Age ref.	Time relationship t+1 (ka)	t+2 (ka)	Distance r d+1 (km)
0	Rangitoto 2	0.50	±0.05	b	-		-
1	Rangitoto 1	0.55	±0.07	b	0.05	-	0.1
2	Mt Wellington	10.00	±0.5	a	9.4	9.5	11.7
3	Purchas Hill	10.90	±0.14	b	0.9	10.3	0.6
4	Pukeiti	15.31	±0.65	a	4.4	5.3	13.4
Rerewhakaaitu (ca. 17.5 ka)							
5	Styaks Swamp	19.10	-	d	3.8	8.2	13.9
6	Green Mt	19.60	±3.3	c	0.5	4.3	0.6
7	Mt Smart	20.08	±0.1	a	0.5	1.0	8.1
8	Waitomokia	20.30	±0.14	a	0.2	0.7	7.6
Okareka (ca. 21.9 ka)							
9	Otuataua	24.20	±0.88	a	3.9	4.1	1.7
10	Mt Robertson	24.26	±0.4	a	0.1	4.0	8.8
11	Pigeon Mt	23.35	±0.35	a	-0.9	-0.8	8.5
12	Motukorea	24.41	±0.29	a	1.1	0.1	6.5
13	Little Rangitoto	24.55	±0.29	a	0.1	1.2	9.1
14	Panmure Basin	25.23	±0.86	a	0.7	0.8	4.8
Oruanui/Kawakawa (ca. 25.4 ka)							
15	Mt Eden	28.03	±0.26	a	2.8	3.5	8.3
16	Te Pou Hawaiki	28.53	-	d	0.5	3.3	0.7
17	Puketutu	29.80	±2.2	a	1.3	1.8	9.3
18	Taylors Hill	30.20	±0.12	a	0.4	1.7	8.0
19	Mt Richmond	30.20	±2.08	a	0.0	0.4	8.0
20	Wiri Mt	30.20	±4.6	c	0.0	0.0	8.5
21	Ash Hill	30.70	-	d	0.5	0.5	1.0
22	Crater Hill	30.40	±0.4	a	-0.3	0.2	4.4
23	Hopua	31.00	-	d	0.6	0.3	6.5
24	Three Kings	31.04	±0.9	a	0.0	0.6	4.6
25	Kohuora	33.71	±1.16	a	2.7	2.7	11.5
26	Mt Hobson	34.20	±0.86	a	0.5	3.2	12.0
27	Mt Victoria	34.78	±2.0	a	0.6	1.1	6.6
28	McLennan Hills	41.30	±1.2	d	6.5	7.1	12.2
29	Mt Cambria	42.30	±11.1	c	1.0	7.5	12.5
30	McLaughlins Hill	48.20	±3.2	c	5.9	6.9	21.5
Pre Rotoehu (ca. 52 ka)							
31	Otara	56.5	-	d	8.3	14.2	8.7
32	Hampton Park	57.0	±16.0	c/d	0.5	8.8	0.5
33	Mangere Mt	59.0	±10.0	a	2.0	2.5	5.4
34	Mangere Lagoon	59.5	-	d	0.5	2.5	0.9
35	One Tree Hill	67.0	±6.0	a	7.5	8.0	8.6
36	Mt St John	75.3	±1.7	c	8.3	15.8	8.2
37	North Head	87.5	±7.6	c	12.2	20.5	6.8
38	Maungetaketake	88.9	±2.4	c	1.4	13.6	19.4

39	Mt Roskill	105.3	±3.1	c	16.4	17.8	9.1
40	Domain	106.0	±4.0	a	0.7	17.1	6.7
41	Grafton	106.5	-	d	0.5	1.2	0.3
42	Mt Albert	117.6	±5.2	c	11.1	11.6	5.6
43	Orakei	126.0	±3.0	a	8.4	19.5	8.6
44	Albert Park	145.0	±2.0	a	19.0	27.4	4.4
45	St Heliers	161.0	±18.0	d	16.0	35.0	8.8
46	Tank Farm	181.0	±1.0	a	20.0	36.0	11.4
47	Onepoto	187.6	-	d	6.6	26.6	0.6
48	Pupuke	193.2	±2.8	c	5.6	12.2	3.3
Undated centres							
	Pukaki	>52.0					
	Pukewairiki	>130					
	Boggust Park	?					
	Cemetery Hill	?					
	Puhinui Craters	?					

elationship d+2 (km)
-
11.8
10.7
12.8
13.4
13.5
8.1
12.3
9.1
7.1
16.8
13.9
8.5
9.1
4.0
7.8
9.9
9.6
9.2
15.8
8.5
3.7
11.5
10.2
7.5
3.2
17.4
7.8
0.4
9.4
16.0
6.5
14.0
6.3
3.3
7.3
14.7
12.7

11.5
15.1
6.4
6.0
3.6
6.3
5.4
5.5
11.4
2.7